uOttawa

L'Université canadienne
Canada's university

FACULTÉ DES ÉTUDES SUPÉRIEURES ET POSTOCTORALES

uOttawa

L'Université canadienne
Canada's university

FACULTY OF GRADUATE AND POSDOCTORAL STUDIES

Chris McDonald
AUTEUR DE LA THÈSE / AUTHOR OF THESIS

M.Sc. (Physics)
GRADE / DEGREE

Department of Physics
FACULTÉ, ÉCOLE, DÉPARTEMENT / FACULTY, SCHOOL, DEPARTMENT

Quantum Dynamics of Multi-Electron Systems in Strong Laser Fields

TITRE DE LA THÈSE / TITLE OF THESIS

Dr. T. Brabec
DIRECTEUR (DIRECTRICE) DE LA THÈSE / THESIS SUPERVISOR

CO-DIRECTEUR (CO-DIRECTRICE) DE LA THÈSE / THESIS CO-SUPERVISOR

EXAMINATEURS (EXAMINATRICES) DE LA THÈSE / THESIS EXAMINERS

Dr. L. Chen

Dr. S. Raymond

Dr. K. Graham

Gary W. Slater
Le Doyen de la Faculté des études supérieures et postdoctorales / Dean of the Faculty of Graduate and Postdoctoral Studies

M A S T E R ' S T H E S I S

Quantum Dynamics of Multi-Electron Systems in Strong Laser Fields

Chris McDonald

Center for Photonics Research, University of Ottawa,

150 Louis Pasteur, Ottawa, ON, K1N 6N5 Canada

Thesis submitted to the Faculty of Graduate and Postdoctoral Studies and the Ottawa-Carleton Institute of Physics in partial fulfillment of the requirements for the M.Sc. degree in Physics

Supervised by:

Thomas Brabec

Center for Photonics Research, University of Ottawa,

150 Louis Pasteur, Ottawa, ON, K1N 6N5 Canada

Ottawa, December 2006

Your file Votre référence
ISBN: 978-0-494-49247-5
Our file Notre référence
ISBN: 978-0-494-49247-5

MASTER'S THESIS

Quantum Dynamics of Multi-Electron Systems in Strong Laser Fields

Chris McDonald

Center for Photonics Research, University of Ottawa, Ottawa, ON, K1N 6N5 Canada

E-mail:

Abstract. The multi-configuration time-dependent Hartree-Fock (MCDTHF) method is a promising new method that can solve the time-dependent Schrödinger equation (TDSE) for a correlated multielectron system. We have written a computer code to solve the MCTDHF equations of motion. This code is highly optimized for speed and makes efficient use of memory. As a first test of the code, we will investigate the ionization dynamics of N_2 in a strong laser-electric field using two active electrons. By examining the final momenta, parallel to the field polarization direction, of the two ionized electrons we are able to determine: i) which laser dressed excited state the second electron was in at the time of ionization and ii) the birth times of the electrons in the field. The results of these calculations provide a means for characterizing the attosecond dynamics of atoms and molecules without using attosecond pulses.

Contents

Acknowledgments

To my fiancée Jamie Kwong: Without your love and support I don't think I could have spent two years and a bit doing my Master's degree.

I would like thank everyone at the Centre for Photonics Reseach at the University of Ottawa. I would especially like to thank my supervisor, Thomas Brabec, for introducing me to this exciting field of research. Without your guidance and insight I don't think the MCTDHF code would have ever got of the ground. As well, I would like to thank Carlos Destefani for all of his help debugging and testing the code and for providing many insightful suggestions. Also, thanks to Thomas Fennel for his help with the MATLAB movies, Suren for the many insightful discussions and Martin and Nabil for helping us deal with uncooperative software. Finally, to all of those who constantly had computer problems (you know who you are) without you I would not have learned so much about Linux.

Chapter 1

Introduction

The study of ionization dynamics is an extremely important endeavour in quantum mechanics [1]. While recent experimental advances have made it possible to directly observe the motion of the valence electrons in atoms and molecules [2], theory continues to lag behind. It is critical for the advancement of attophysics to develop a sound theoretical understanding of how multielectron systems behave when under the influence of a strong laser field [3]; this requires a time-dependent formulation of quantum mechanics. Currently, directly solving the time-depenent Schrödinger equation (TDSE) for a correlated multielectron system is not computationally feasible. For instance, consider an atom, in the Born-Oppenheimer approximation, with five active electrons. For a 3-D calculation using 10 points on each axis, the amount of memory alone needed to represent the quantum mechanical wave would be 10^{15} complex numbers. Assuming that each complex number requires 16 bytes, the total amount of memory needed would be 1.6×10^{16} bytes; that is, 1.6×10^{4} terabytes. Thus, in order to perform calculations on multielectron systems approximate methods need to be used.

The TDSE for multielectron systems has, for the most part, been solved by assuming that only the most weakly bound electron is involved in the ionization dynamics. This is known as the single active electron approximation (SAE). While sufficient for simple systems, experiments performed over the last few years have shown that the SAE approximation is inadaquate for describing more complex molecules [4, 5, 6].

There exist several approaches that go beyond the SAE approximation and attempt to examine the physical processes involved in the interaction of strong laser pulses with multielectron systems. In chapter 2 we will discuss some these methods and explain some of their downsides for time-dependent calculations on correlated multielectron systems. We will also discuss the multi-configuration time-dependent Hartree (MCTDH) method used for the propagation of wave packets and we will give a brief introduction to the multi-configuration time-dependent Hartree-Fock (MCTDHF) method.

In chapter 3 we will give a detailed introduction to the MCTDHF method and we will show a full derivation of the MCTDHF equations of motion. As well, we will briefly discuss some of the more complicated aspects that will need to be considered to perform any calculation. In particular we will show how the calculation of the mean-field operator can be greatly simplified.

Chapter 4 will discuss how we actually solve the MCTDHF equations of motion. We will present a highly optimized computer code that is capable of solving the TDSE for small multi-electron systems in one and two dimensions. We will provide a detailed description of how the code solves the MCTDHF equations of motion. As well, we show how some of the larger portions of the calculation can be scaled down.

In chapter 5 we will use the MCTDHF code to solve the TDSE for an N_2 molecule in a strong laser field. Here we will investigate the ionization dynamics of N_2 when the molecular axis is aligned both perpendicular and parallel to the polarization of the laser field. We will also provide an explanation of the results using a simple classical model and present results that do not appear classically. Finally, in chapter 6 we summarize the results.

Chapter 2

Background on numerical solutions of the TDSE

This chapter will provide some background information on the most widely used methods to solve the TDSE. We will provide the basic principles of these methods and discuss some of their drawbacks when solving the TDSE for a correlated multielectron system in the presence of a strong laser field. We will also briefly introduce the multi-configuration time-depedent Hartree-Fock approach and provide insight into some areas of physics for which this approach can be extemely useful.

2.1 The Hartree-Fock approach and configuration interaction

The Hartree-Fock (HF) approach assumes that each electron is affected by the nuclear potential and the average repulsive interactions between the other electrons [7]. Each electron occupies a spin-orbital represented by a single particle function, φ_i. In the HF approach, the quantum mechanical wave function, for an f electron system, is approximated by a single Slater determinant as,

$$\Psi = \frac{1}{\sqrt{f!}} \sum_{\pi} sgn(\pi) \prod_{i=1}^{f} \varphi_{\pi(i)}(x_i) \tag{2.1}$$

where π runs through all permutations and $sgn(\pi)$ is $+1$ for even permutations and -1 for odd permuations. The x_i represents both spatial and spin coordinates for the i^{th} particle.

In HF the best approximation of the wave function is found by minimizing the energy as a functional of the spin-orbitals (φ_i) subject to the constraint that the spin-orbitals remain orthonormal. That is, for the functional $E[\{\varphi_i\}]$, we wish to find the set $\{\varphi_i\}$, with the constraints $\langle\varphi_i|\varphi_j\rangle = \delta_{ij}$, such that for the first variation of E we have $\delta E = 0$.

Essentially there are two forms of HF; restricted and unrestricted. Restricted HF assumes that each shell is closed; ie: there are an even number of electrons. For a given shell it is only the spin part of the spin-orbital function that differs for each electron. In unrestricted HF this constraint is lifted.

For time-dependent problems the HF approach can be extended to the time-dependent HF approach (TDHF) [8, 9, 10, 11, 12, 13, 14]. Here the ansatz used to approximate the wave function is given by,

$$\Psi(t) = \frac{1}{\sqrt{f!}} \sum_{\pi} sgn(\pi) \prod_{i=1}^{f} \varphi_{\pi(i)}(x_i; t) \tag{2.2}$$

The only difference from equation (2.1) being that the spin orbitals are now time-dependent. The TDHF equations of motion can then be found by performing the variation [1] [12],

$$i\langle\delta\Psi|\partial_t\Psi\rangle = \langle\delta\Psi|H|\Psi\rangle \tag{2.3}$$

and keeping the spin-orbitals orthonormal [2]. The TDHF equations, in standard form, come out to be,

$$i\partial_t\varphi_i = H^{(1)}\varphi_i + \sum_j [V_{jj}\varphi_i - V_{ji}\varphi_j] \tag{2.4}$$

where $V_{ji} = \langle\varphi_j|H^{(2)}|\varphi_i\rangle$, $H^{(1)}$ is the one body operator and $H^{(2)}$ is the two body part of the Hamiltonian [15].

The TDHF method's problems lie in the fact that it is a single determinant approach and that the interaction of the electrons is treated in an average way. As such, it fails to properly take into account electron correlation.

We end this section by briefly discussing the configuration interaction (CI) approach [7, 16, 17]. Since the HF approach is only a single determinant approach and does not take into account electron correlation the next logical step is to expand the wave function using many Slater dererminants. In CI the wave function is written using the ansatz.

$$\Psi = \sum_{J=0}^{N} A_J \Phi_J \tag{2.5}$$

where J is a set of subscripts ,$\{j_i\}$, Φ_J is the Slater determinant formed from all permutations of $\varphi_{j_1}\cdots\varphi_{j_f}$ and A_J is the weighting coefficient for the Slater determinant J.

In CI, the A_J coefficients are optimized to give the best approximation of the wave function for the system. This method appears simple in nature but often requires large numbers of Slater determinants produced from complex basis sets. Often the number of configurations required becomes umanageably large.

2.2 Time-dependent density functional theory

Another common approach to solving the Schrödinger equation is density functional theory (DFT). DFT is built from the Hohenberg-Kohn (HK) theorem [18] which we now state.

The Hohenberg-Kohn Theorem: The external potential U for a bound system of interacting electrons is uniquely determined, up to an additive constant, by the ground-state density ρ.

The HK theorem implies that there exists a map G such that G: $U \to \rho$ is invertible. Since the kinetic energy (T) and Coulomb repulsion (V) operators are universal to any system the Hamiltonian H is uniquely determined by U. Thus, ρ determines the Hamiltonian of the system and hence implicitly determines all physical properties that can be obtained from H. The exact ground state density function is found when the energy functional,

$$E_U[\rho] := F[\rho] + \int U(\boldsymbol{r})\rho(\boldsymbol{r})d\boldsymbol{r} \tag{2.6}$$

[1] This variation principle is actually the Dirac-Frenkel principle which will later be used to derive the MCTDHF equations of motion.

[2] In general the spin-orbitals need not be orthonormal; however, this simplifies the TDHF equations.

is minimized, where F is the universal functional $F[\rho] = \langle\Psi|(T+V)|\Psi\rangle$. This is known as the HK variational principle [19] and is expressed as,

$$E_g = min_{\tilde{\rho}} E_U[\tilde{\rho}] \tag{2.7}$$

where E_g is the ground state energy of the system and $\tilde{\rho}$ is a trial density function.

Using the HK variational principle it was shown that the system of interacting particles takes on the form of a system of non-interacting particles moving in an effective potential U_{eff} [20] given by,

$$U_{eff} := U + \int \frac{\rho(\boldsymbol{r}\prime)}{|\boldsymbol{r}-\boldsymbol{r}\prime|d\boldsymbol{r}\prime} + U_{xc} \tag{2.8}$$

where U_{xc} is the local exchange-correlation potential [19]; this is a functional of the density ρ. The role of the functional $U_{xc}[\rho]$, as its name states, is to take into account the exchange and correlation effects. The minimizing density can then be found by solving the single particle Schrödinger equations,

$$\left(-\frac{1}{2}\nabla^2 + U_{eff}\right)\varphi_i = E_i\varphi_i \tag{2.9}$$

where U_{eff} is defined above and the density can be determined from,

$$\rho = \sum_i |\varphi_i|^2 \tag{2.10}$$

These are known as the Kohn-Sham (KS) equations and provide a practical way of calculating the electron density.

Density functional theory has been extended to time-dependent problems; this is known as time-dependent density functional theory (TDDFT). A theorem analagous to the HK theorem has been developed for time dependent systems [21]. This theorem, which is known as the Runge-Gross (RG) theorem, states:

The Runge-Gross Theorem: For every single-particle potential U that has a Taylor series in the neighbourhood of $t = t_0$ the invertible map G: $U \rightarrow \rho$ is defined by solving the TDSE with a fixed intial state and calculating the coresponding density.

The RG theorem in fact holds for piecewise analytic potentials as well and is a special case of a more general theory [22]. In this case the time-dependent density for a given system can always be obtained by an external potential in a system with a different particle-particle interaction, provided that the initial states of the system have the same intial density and the same initial momentum. Also, analagous to the HK variational principle, it is shown that the action integral,

$$A = \int_{t_0}^{t_1} dt\, \langle\Psi(t)|i\partial_t - H(t)|\Psi(t)\rangle \tag{2.11}$$

can be written as the functional of the density,

$$A[\rho] := F[\rho] - \int_{t_0}^{t_1} dt \int d\boldsymbol{r} U(\boldsymbol{r};t)\rho(\boldsymbol{r};t) \tag{2.12}$$

where $F[\rho]$ is the universal functional of density given by,

$$F[\rho] = \int_{t_0}^{t_1} dt \, \langle \Psi(t) | i\partial_t - T - V | \Psi(t) \rangle \tag{2.13}$$

The density can then be computed using equation (2.10) by solving the single-particle TDSE [21, 23],

$$i\partial_t \varphi_i = \left[-\frac{1}{2}\nabla^2 + U_{eff} \right] \varphi_i \tag{2.14}$$

where U_{eff} is the time-dependent analogue of that in equation (2.8).

One major drawback to TDDFT is the difficulty associated with the determination of the exchange-correlation functional. Proposed methods to construnct U_{xc} [24, 25] are extremely complicated and it is difficult to gauge their accuracy. Another major draw back of TDDFT is that it provides only the density of the system and not the quantum mechanical wave function. As well, DFT has encountered many other problems [26, 27, 28]. One of these [26] being a severe fundamental problem in which the entire history of the density enters into the exchange-correlation term. This can cause ambiguities when representing excited states. Much like TDHF, TDDFT fails to properly account for electron correlation.

2.3 The multiconfiguration time-dependent Hartree method

The multiconfiguration time-dependent Hartree (MCTDH) method [29] is a multi-configuration method designed primarily for the propagation of wave packets. It is on this method that the multi-configuration time-dependent Hartree-Fock (MCTDHF) method, the main topic of this document, is based. As such, we will present a brief overview of MCTDH.

In the MCTDH approach the wave function Ψ for a system with f degrees of freedom is approximated by a linear combination of Hartree products built using a basis of time-dependent single-particle functions $\varphi_{j_i}^{(i)}$ for each degree of freedom i [30]. The wave function Ψ is then represented as,

$$\Psi(\boldsymbol{q}_1, \ldots, \boldsymbol{q}_f; t) = \sum_{j_1=1}^{n_1} \cdots \sum_{j_f=1}^{n_f} A_{j_1 \ldots j_f}(t) \varphi_1^{(1)}(\boldsymbol{q}_1; t) \ldots \varphi_f^{(f)}(\boldsymbol{q}_f; t) \tag{2.15}$$

where $A_{j_1 \ldots j_f}(t)$ are the time-dependent expansion coefficients and n_i is the number of expansion functions for the $i^t h$ degree of freedom.

In order to obtain a unique representation of the wave function, constraints are placed on the single particle functions; these are,

$$\left\langle \varphi_{j_k}^{(i)}(0) \middle| \varphi_{j_l}^{(i)}(0) \right\rangle = \delta_{kl} \tag{2.16}$$

$$\left\langle \varphi_{j_k}^{(i)}(t) \middle| \dot{\varphi}_{j_l}^{(i)}(t) \right\rangle = -i \left\langle \varphi_{j_k}^{(i)}(t) \middle| g^{(i)} \middle| \varphi_{j_l}^{(i)}(t) \right\rangle \tag{2.17}$$

where g is a single-particle, Hermitian operator.

The equations of motion for the single-particle functions and the time-dependent expansion coefficients can be determined by applying the Dirac-Frenkel variational principle [31, 32, 33] to

the MCTDH wave function and using constraints (2.16) and (2.17). After a lengthy derivation, the equations of motion for the expansion coefficients are determined to be,

$$i\dot{A}_J = \sum_L \langle \Phi_J | H | \Phi_L \rangle A_L - \sum_{i=1}^{f} \sum_{k=1}^{n_i} g^{(i)}_{j_i k} A_{J^i_k} \tag{2.18}$$

where $A_J = A_{j_1 \ldots j_f}$, $\Phi_J = \prod_{i=1}^{f} \varphi^{(i)}_{j_i}$, $g^{(i)}_{jk} = \left\langle \varphi^{(i)}_j \middle| g^{(i)} \middle| \varphi^{(i)}_k \right\rangle$ and $A_{J^i_k} = A_{j_1 \ldots j_{i-1} k j_{i+1} \ldots j_f}$. The equations of motions for the single particle functions are determined to be,

$$\mathrm{i}\dot{\boldsymbol{\varphi}}^{(i)} = g^{(i)} \mathbf{1}_{n_i} \boldsymbol{\varphi}^{(i)} + (1 - \mathrm{P}^{(i)}) [(\boldsymbol{\rho}^{(i)})^{-1} \langle \mathrm{H} \rangle^{(i)} g^{(i)} \mathbf{1}_{n_i}] \boldsymbol{\varphi}^{(i)} \tag{2.19}$$

where $\boldsymbol{\varphi}^{(i)} = (\varphi^{(i)}_1 \ldots \varphi^{(i)}_f)^T$, $\mathrm{P}^{(i)}$, the projector onto the space spanned by the single-particle functions for the i^{th} degree of freedom, is given by,

$$\mathrm{P}^{(i)} = \sum_{k=1}^{n_i} \left| \varphi^{(i)}_k \right\rangle \left\langle \varphi^{(i)}_k \right| \tag{2.20}$$

and the mean field operator $\langle \mathrm{H} \rangle^{(i)}$ and density matrix $\rho^{(i)}$ for the i^{th} degree of freedom are defined by,

$$\langle \mathrm{H} \rangle^{(i)}_{jk} = \left\langle \Psi^{(i)}_j \middle| \mathrm{H} \middle| \Psi^{(i)}_k \right\rangle \tag{2.21}$$

$$\rho^{(i)}_{jk} = \left\langle \Psi^{(i)}_j \middle| \Psi^{(i)}_k \right\rangle \tag{2.22}$$

where $\Psi^{(i)}_j$ is the single hole function for the i^{th} degree of freedom defined by,

$$\Psi^{(i)}_k = \sum_{j_1} \cdots \sum_{j_{i-1}} \sum_{j_{i+1}} \cdots \sum_{j_f} A_{j_1 \ldots j_{i-1} k j_{i+1} \ldots j_f} \varphi^{(1)}_{j_1} \cdots \varphi^{(i-1)}_{j_{i-1}} \varphi^{(i+1)}_{j_{i+1}} \cdots \varphi^{(f)}_{j_f} \tag{2.23}$$

The MCTDH approach has been applied to a wide variety of problems. Some of these include photo-excitation [34, 35, 36], photo-dissociation [37, 38, 39] and inelastic surface scattering [40, 41, 42] to name a few. A full list of applications of MCTDH can be seen in reference [30].

2.4 The multiconfiguration time-dependent Hartree-Fock approach

In this section we will briefly describe the multiconfiguration time-dependent Hartree-Fock (MCTDHF) [43] approach; a detailed discussion of MCTDHF will be presented in the next chapter. This approach is designed to solve the TDSE for a multielectron system with a time-dependent Hamiltonian. The MCTDHF method is a generalization of the time-dependent CI approach. In addition to optimizing the time-dependent expansion coefficients, MCTDHF also optimizes the set of (time-dependent) expansion functions. By optimizing the expansion functions it requires significantly less configurations to approximate the wave function and thus makes it more feasible to be used for calculations on multielectron systems. The MCTDHF ansatz is based on the ansatz used in the MCTDH approach. It differs from MCTDH by restricting the solution to be totally antisymmetric and adding exchange symmetry to the time-dependent Hamiltonian. The equations of motion for the time-dependent expansion coefficients and the expansion functions

are derived using a variational principal and give similar equations to those for the MCTDH approach.

MCTDHF is currently the only approach that is capable of solving the TDSE for a multi-electron system and still take into account electron correlation. As such there is a wide spectrum of possibilities available where MCTDHF can be of great use. Some of these include:

(i) *Intense x-ray atom interaction* - High intensity x-ray pulses with pulse durations of about 100 as - 100fs can be created. These sources have great potential to investigate the structure of biomolecules. Since these molecules will be destroyed quickly ($\approx 10fs$) by the radiation a sound theoretical understanding of the interaction between intense x-ray radiation and matter is of supreme importance.

(ii) *Laser driven impact ionization in plasmas* - Impact ionization, where a free electron collides with a nucleus and causes one or more bound electrons to be set free, is an important ionization process in plasmas. Plasmas are often created by intense laser pulses. Experiments [44, 45, 46] and classical calculations [47, 48] that have been done show that the laser field does indeed have a significant effect on impact ionization; however, the capability to do a quantum mechanical calculation for this problem is not yet available. MCTDHF has the capability to calculate the enhanced cross section of $He^+ + e^- \rightarrow He^{2+} + 2e^-$, with the possibility of extending these calculations to more complex atoms.

(iii) *Nanophysics* - Quantum dots are extremely important to quantum computing; they may provide one possible avenue to the realization of qubits [49]. As well, quantum dots and large molecules are used in nanotechnology to create the smallest switches and transistors [50, 51]. Here, MCTDHF provides a means for theoretical investigation.

Recently the MCTDHF method has been successfully tested using 1-D systems [1, 52, 53, 54]. However, calculations in 2-D and 3-D have yet to be considered. The code presented in chapter 4 is capable of doing calculations for small 2-D systems on a single processor. This code also has the capability of being generalized to 3-D with minor modification.

2.5 The time-dependent quantum Monte-Carlo approach

We end this chapter by discussing one more approach currently in development - time-dependent quantum Monte-Carlo (TDQMC) [55]. Through the use of quantum Monte Carlo (QMC) methods [56], it is possible to calculate the ground state wave function of quantum mechanical systems. QMC methods calculate the ground state wave function by exploiting the similarity between the generalized diffusion stocastic motion of Brownian particles (or "walkers") and the solution of the Schrödinger equation in imaginary time. The wave function is found by following the motion of the walker in configuration space.

In the TDQMC approach, a complex, time-depenent, guide function is attached to each walker. This guide function then evolves in time according to the TDSE along with the trajectory of the corresponding walker. Recently, this method has been used to some avail for modeling 1-D hydrogen and 1-D helium atoms [57, 58]. In TDQMC an ensemble of N walkers is used to represent each electron. The guide functions for the k^{th} walker and i^{th} electron φ_i^k then evolve according to,

$$i\partial_t \varphi_i^k(\boldsymbol{r}_i;t) = \left[-\frac{1}{2}\nabla_i^2 + U(\boldsymbol{r}_i) + \sum_{j\neq i}^{f} V(\boldsymbol{r}_i - \boldsymbol{r}_j^k(t)) + i\vec{A}(t)\cdot\vec{\nabla}_i\right]\varphi_i^k(\boldsymbol{r}_i;t) \qquad (2.24)$$

where U is the external potential, V is the electron-electron potential, f is the number of electrons, $i \in \{1, \ldots, f\}$, $k \in \{1, \ldots, N\}$, A is the vector potential of the laser field and $\boldsymbol{r}_j^k(t)$ is the trajectory of the k^{th} walker for the j^{th} electron ensemble. The trajectory of the walkers is described by the de Broglie-Bohm wave relation [59]; this is given by,

$$\frac{d\boldsymbol{r}_i^k(t)}{dt} = Im\left[\frac{\nabla_i \Psi(\boldsymbol{r}_1, \ldots, \boldsymbol{r}_f, t)}{\Psi(\boldsymbol{r}_1, \ldots, \boldsymbol{r}_f, t)}\right]_{\boldsymbol{r}_j = \boldsymbol{r}_j^k(t)\ \forall j} - \vec{A}(t) \tag{2.25}$$

where Ψ is represented by a single Slater determinant or as a sum of Slater determinants made up from the guiding functions. Equations (2.24) and (2.25), governing the motion of the guide functions and the walkers, form a set of self-contained equations. While there is no exchange term in equation (2.24), this accounted for in equation (2.25).

Chapter 3

The multi-configuration time-dependent Hartree-Fock method

This chapter will serve as a detailed introduction to the multi-configuration time-dependent Hartree-Fock method (MCTDHF). Here we will introduce the ansatz used to approximate the quantum mechanical wave function and provide a detailed derivation of the MCTDHF working equations. As well, we will discuss where the major computational work loads will appear when solving the MCTDHF equations.

3.1 MCTDHF Theory

The MCTDHF method is an approximate method that is capable of solving the time-dependent Schrödinger equation (TDSE)

$$i\partial_t \Psi(\boldsymbol{q}_1, \ldots, \boldsymbol{q}_f; t) = \mathrm{H}\Psi(\boldsymbol{q}_1, \ldots, \boldsymbol{q}_f; t) \tag{3.1}$$

for a system with f electrons in a time dependent Hamiltonian. The coordinates $\boldsymbol{q}_i$ represent the three spatial coordinates, $\boldsymbol{x}_i$, and the spin coordinate, s_i, for the i^{th} electron. Here equation (3.1) is presented in atomic units; unless otherwise stated, atomic units will be used throughout this document [1]. The goal of MCTDHF is to solve (3.1) in a reasonable amount of time and with a relatively low computation cost while still taking into account electron correlation.

3.1.1 The MCTDHF ansatz

In MCTDHF the exact solution to (3.1) is approximated using a set of n time-dependent spin orbitals $\{\varphi_i(\boldsymbol{q}; t)\}$ and a set of time-dependent linear expansion coefficients $A_{j_1 \ldots j_f}(t)$. In the formal mathematical sense we say that the wave function is approximated and a manifold $\mathcal{M}$ of square integrable functions. Thus we write the normalized MCTDHF wave function as

$$\Psi(\boldsymbol{q}_1, \ldots, \boldsymbol{q}_f; t) \approx \sum_{j_1=1}^{n} \ldots \sum_{j_f=1}^{n} A_{j_1 \ldots j_f}(t) \varphi_{j_1}(\boldsymbol{q}_1; t) \ldots \varphi_{j_f}(\boldsymbol{q}_f; t). \tag{3.2}$$

In order to preserve the anti-symmetry of the wave function we require that the linear expansion coefficients be anti-symmetric with respect to the exchange of any two indices; that is,

$$A_{j_1 \ldots j_k \ldots j_l \ldots j_f} = -A_{j_1 \ldots j_l \ldots j_k \ldots j_f}. \tag{3.3}$$

[1] For conversion between SI and atomic units, see appendix A.

This leaves only $\binom{n}{f}$ independent expansion coefficients. In the limit $n = f$ we retrieve time-dependent Hartree-Fock approximation. The benefit to MCTDHF is that it scales linearly with the number of spin-orbitals and as $\binom{n}{f}$ with the expansion coefficients.

3.1.2 Constraints

The ansatz in equation (3.2) is not unique. In fact it is invariant under the transformations

$$\varphi_j \rightarrow \widetilde{\varphi}_j = \sum_{k=1}^{n} B_{jk}\varphi_k \tag{3.4}$$

$$A_{j_1\ldots j_f} \rightarrow \widetilde{A}_{j_1\ldots j_f} = \sum_{k_1=1}^{n}\cdots\sum_{k_f=1}^{n} B^{-1}_{j_1k_1}\cdots B^{-1}_{j_fk_f}A_{k_1\ldots k_f} \tag{3.5}$$

where B(t) can be any invertible $n \times n$ matrix [52]. In order to restrict our choice of B(t) and ensure orthonormality of the spin orbital functions, we use the following constraints:

$$\langle\varphi_i(0)|\varphi_j(0)\rangle = \delta_{ij}, \tag{3.6}$$

$$\langle\varphi_i(t)|\dot{\varphi}_j(t)\rangle = -\mathrm{i}g_{ij} \tag{3.7}$$

where $g(t)$ is an arbitrary, single particle Hermitian operator and $g_{ij} = \langle\varphi_i(t)|\mathrm{g}(t)|\varphi_j(t)\rangle$. The actual choice of $g(t)$ will be discussed later.

3.1.3 The MCTDHF equations of motion

Before we begin the derivations of the MCTDHF equations of motion we first define the single-hole function

$$\left|\Psi^{(l)}\right\rangle := \langle\varphi_l|\Psi\rangle = \sum_{j_2=1}^{n}\ldots\sum_{j_f=1}^{n} A_{lj_2\ldots j_f}\left|\varphi_{j_2}\ldots\varphi_{j_f}\right\rangle. \tag{3.8}$$

As well, we define the density matrix and the mean field operator as,

$$\rho_{jl} := \left\langle\Psi^{(j)}\middle|\Psi^{(l)}\right\rangle = \sum_{j_2=1}^{n}\cdots\sum_{j_f=1}^{n} A^{*}_{jj_2\ldots j_f}A_{lj_2\ldots j_f} \tag{3.9}$$

$$\langle\mathrm{H}\rangle_{jl} := \left\langle\Psi^{(j)}\middle|\mathrm{H}\middle|\Psi^{(l)}\right\rangle. \tag{3.10}$$

Furthermore, we define the projector onto the subspace spanned by the spin orbital functions as,

$$P := \sum_{l}|\varphi_l\rangle\langle\varphi_l|. \tag{3.11}$$

From this point on all summation over indices is done from 1 to n unless otherwise indicated.

The derivation of the MCTDHF equations of motion begins with the Dirac-Frenkel variational principle

$$\langle\delta\Psi|i\partial_t - H|\Psi\rangle = 0 \tag{3.12}$$

where $\delta\Psi$ is an element of the tangent space $T_\Psi\mathcal{M}$ at Ψ. That is, for each time we require that the residual $(\mathrm{i}\partial_t - H)|\Psi\rangle$ be orthogonal to $T_\Psi\mathcal{M}$. This ensures that $\mathrm{i}\dot{\Psi}(\boldsymbol{x}_1 \dots \boldsymbol{x}_f; t)$, within the ansatz, is closest to its true value [52, 60].

Performing the variation in (3.12) we get,

$$\delta\Psi = \sum_{j_1\dots j_f} \delta A_{j_1\dots j_f} \varphi_{j_1}\cdots\varphi_{j_f} + \sum_{j_1\dots j_f} A_{j_1\dots j_f} \sum_{i=1}^{f} \varphi_{j_1}\cdots\delta\varphi_{j_i}\cdots\varphi_{j_f}. \tag{3.13}$$

Substituting (3.13) into equation (3.12) gives,

$$\begin{aligned}
&\mathrm{i}\sum_{j_1\dots j_f}\left\langle\varphi_{j_1}\cdots\varphi_{j_f}\middle|\dot{\Psi}\right\rangle\delta A^*_{j_1\dots j_f} + \mathrm{i}\sum_{i=1}^{f}\sum_{j_1\dots j_f} A_{j_1\dots j_f}\left\langle\varphi_{j_1}\cdots\varphi_{j_{i-1}}\varphi_{j_{i+1}}\cdots\varphi_{j_f}\middle|\dot{\Psi}\right\rangle\delta\varphi^*_{j_i}\\
&= \sum_{j_1\dots j_f}\langle\varphi_{j_1}\cdots\varphi_{j_f}|H|\Psi\rangle\,\delta A^*_{j_1\dots j_f} + \sum_{i=1}^{f}\sum_{j_1\dots j_f} A_{j_1\dots j_f}\langle\varphi_{j_1}\cdots\varphi_{j_{i-1}}\varphi_{j_{i+1}}\cdots\varphi_{j_f}|H|\Psi\rangle\,\delta\varphi^*_{j_i}
\end{aligned} \tag{3.14}$$

where $\dot{\Psi}$ is given by,

$$\left|\dot{\Psi}\right\rangle = \sum_{j_1\dots j_f}\dot{A}_{j_1\dots j_f}|\varphi_{j_1}\cdots\varphi_{j_f}\rangle + \sum_{j_1\dots j_f} A_{j_1\dots j_f}\sum_{i=1}^{f}|\varphi_{j_1}\cdots\dot{\varphi}_{j_i}\cdots\varphi_{j_f}\rangle. \tag{3.15}$$

From equation (3.14) we get the following set of equations:

$$\mathrm{i}\left\langle\varphi_{j_1}\dots\varphi_{j_f}\middle|\dot{\Psi}\right\rangle = \langle\varphi_{j_1}\dots\varphi_{j_f}|H|\Psi\rangle \tag{3.16}$$

$$\mathrm{i}\left\langle\Psi^{(k)}\middle|\dot{\Psi}\right\rangle = \left\langle\Psi^{(k)}\middle|H\middle|\Psi\right\rangle. \tag{3.17}$$

To obtain the equation of motion for the linear expansion coefficients we substitute equation (3.15) into equation (3.16) and rearrange to get,

$$\begin{aligned}
\mathrm{i}\dot{A}_{j_1\dots j_f} &= \sum_{l_1\dots l_f} A_{l_1\dots l_f}\langle\varphi_{j_1}\dots\varphi_{j_f}|H|\varphi_{l_1}\dots\varphi_{l_f}\rangle\\
&\quad -\mathrm{i}\sum_{i=1}^{f}\sum_{l_1\dots l_f} A_{l_1\dots l_f}\langle\varphi_{j_1}\dots\varphi_{j_f}|\varphi_{l_1}\cdots\dot{\varphi}_{l_i}\cdots\varphi_{l_f}\rangle.
\end{aligned} \tag{3.18}$$

Next we need to obtain the equations of motion for the spin orbital functions. To do this, we first note that Ψ can be written as,

$$|\Psi\rangle = \sum_{k=1}^{n}\left|\varphi_k\Psi^{(k)}\right\rangle \tag{3.19}$$

Then subbing (3.19) into the right hand side of equation (3.17) we have,

$$\begin{aligned}
\left\langle\Psi^{(k)}\middle|H\middle|\Psi\right\rangle &= \sum_l|\varphi_l\rangle\left\langle\Psi^{(k)}\middle|H\middle|\Psi^{(l)}\right\rangle\\
&= \sum_l\langle H\rangle_{kl}|\varphi_l\rangle.
\end{aligned} \tag{3.20}$$

To obtain the left hand side of (3.17) we put (3.8) and (3.15) into (3.17) to get,

$$\mathrm{i}\left\langle \Psi^{(k)}\middle|\dot{\Psi}\right\rangle = \mathrm{i}\sum_{j_2\dots j_f}\sum_{l_1\dots l_f} A^*_{kj_2\dots j_f}\dot{A}_{l_1\dots l_f}\left\langle \varphi_{j_2}\cdots\varphi_{j_f}\middle|\varphi_{l_1}\cdots\varphi_{l_f}\right\rangle$$

$$+\mathrm{i}\sum_{j_2\dots j_f}\sum_{l_1\dots l_f} A^*_{kj_2\dots j_f}A_{l_1\dots l_f}\sum_{i=1}^{f}\left\langle \varphi_{j_2}\cdots\varphi_{j_f}\middle|\varphi_{l_1}\cdots\dot{\varphi}_{l_i}\cdots\varphi_{l_f}\right\rangle . \tag{3.21}$$

Now using constraint (3.6) in the first part of the right hand side of (3.21) and splitting the sum over i into $i=1$ and $i\geq 2$ we get,

$$\mathrm{i}\left\langle \Psi^{(k)}\middle|\dot{\Psi}\right\rangle = \mathrm{i}\sum_{l}|\varphi_l\rangle\sum_{j_2\dots j_f}A^*_{kj_2\dots j_f}\dot{A}_{lj_2\dots j_f} + \mathrm{i}\sum_{l}|\dot{\varphi}_l\rangle\sum_{j_2\dots j_f}A^*_{kj_2\dots j_f}A_{lj_2\dots j_f}$$

$$+\mathrm{i}\sum_{l}|\varphi_l\rangle\sum_{j_2\dots j_f}\sum_{l_2\dots l_f}A^*_{kj_2\dots j_f}A_{ll_2\dots l_f}\sum_{i=2}^{f}\left\langle \varphi_{j_2}\cdots\varphi_{j_f}\middle|\varphi_{l_2}\cdots\dot{\varphi}_{l_i}\cdots\varphi_{l_f}\right\rangle . \tag{3.22}$$

Next we substitute (3.18) into (3.22) and use definition (3.9) to get,

$$\mathrm{i}\left\langle \Psi^{(k)}\middle|\dot{\Psi}\right\rangle = \sum_{l}|\varphi_l\rangle\langle\varphi_l|\sum_{m}|\varphi_m\rangle\sum_{j_2\dots j_f}\sum_{l_2\dots l_f}A^*_{kj_2\dots j_f}A_{ml_2\dots l_f}\left\langle \varphi_{j_2}\cdots\varphi_{j_f}\middle|H\middle|\varphi_{l_2}\cdots\varphi_{l_f}\right\rangle$$

$$-\mathrm{i}\sum_{l}|\varphi_l\rangle\sum_{j_2\dots j_f}\sum_{l_1\dots l_f}A^*_{kj_2\dots j_f}A_{l_1\dots l_f}\sum_{i=1}^{f}\left\langle \varphi_l\varphi_{j_2}\cdots\varphi_{j_f}\middle|\varphi_{l_1}\cdots\dot{\varphi}_{l_i}\cdots\varphi_{l_f}\right\rangle$$

$$+\mathrm{i}\sum_{l}\rho_{kl}|\dot{\varphi}_l\rangle + \mathrm{i}\sum_{l}|\varphi_l\rangle\sum_{j_2\dots j_f}\sum_{l_2\dots l_f}A^*_{kj_2\dots j_f}A_{ll_2\dots l_f}\sum_{i=2}^{f}\left\langle \varphi_{j_2}\cdots\varphi_{j_f}\middle|\varphi_{l_2}\cdots\dot{\varphi}_{l_i}\cdots\varphi_{l_f}\right\rangle \tag{3.23}$$

Now using the definitions (3.9) – (3.11) and constraint(3.6) and, as in (3.22), splitting the sum over i we get,

$$\mathrm{i}\left\langle \Psi^{(k)}\middle|\dot{\Psi}\right\rangle = P\sum_{l}\langle H\rangle_{kl}|\varphi_l\rangle + \mathrm{i}\sum_{l}\rho_{kl}|\dot{\varphi}_l\rangle - \mathrm{i}\sum_{l}|\varphi_l\rangle\sum_{m}\rho_{km}\langle\varphi_l|\dot{\varphi}_m\rangle$$

$$-\mathrm{i}\sum_{l}|\varphi_l\rangle\sum_{j_2\dots j_f}\sum_{l_2\dots l_f}A^*_{kj_2\dots j_f}A_{ll_2\dots l_f}\sum_{i=2}^{f}\left\langle \varphi_{j_2}\cdots\varphi_{j_f}\middle|\varphi_{l_2}\cdots\dot{\varphi}_{l_i}\cdots\varphi_{l_f}\right\rangle$$

$$+\mathrm{i}\sum_{l}|\varphi_l\rangle\sum_{j_2\dots j_f}\sum_{l_2\dots l_f}A^*_{kj_2\dots j_f}A_{ll_2\dots l_f}\sum_{i=2}^{f}\left\langle \varphi_{j_2}\cdots\varphi_{j_f}\middle|\varphi_{l_2}\cdots\dot{\varphi}_{l_i}\cdots\varphi_{l_f}\right\rangle . \tag{3.24}$$

Substituting equations (3.20) and (3.24) into (3.17) and noting that the last two terms in equation (3.24) cancel gives,

$$\sum_{l}\langle H\rangle_{kl}|\varphi_l\rangle = P\sum_{l}\langle H\rangle_{kl}|\varphi_l\rangle + i\sum_{l}\rho_{kl}|\dot{\varphi}_l\rangle - \mathrm{i}\sum_{l}|\varphi_l\rangle\sum_{m}\rho_{km}\langle\varphi_l|\dot{\varphi}_m\rangle . \tag{3.25}$$

Defining $\boldsymbol{\varphi} := (|\varphi_1\rangle,\dots,|\varphi_f\rangle)^T$ and $\dot{\boldsymbol{\varphi}} := (|\dot{\varphi}_1\rangle,\dots,|\dot{\varphi}_f\rangle)^T$ we have,

$$\langle \mathrm{H}\rangle\,\boldsymbol{\varphi} = \mathrm{P}\,\langle \mathrm{H}\rangle\,\boldsymbol{\varphi} + \mathrm{i}\boldsymbol{\rho}\dot{\boldsymbol{\varphi}} - \mathrm{P}\boldsymbol{\rho}\boldsymbol{g}\boldsymbol{\varphi}. \tag{3.26}$$

Finally, using constraint (3.7) in equation (3.18) and acting $\boldsymbol{\rho}^{-1}$ on the right of (3.26) and rearranging we get the following set of non-linear equations:

$$\mathrm{i}\dot{A}_{j_1\ldots j_f} = \sum_{l_1\ldots l_f} A_{l_1\ldots l_f} \left\langle \varphi_{j_1}\ldots\varphi_{j_f}\middle|H\middle|\varphi_{l_1}\ldots\varphi_{l_f}\right\rangle - \sum_{i=1}^{f}\sum_{k} g_{j_i k} A_{j_1\ldots j_{i-1}kj_{i+1}\ldots j_f} \tag{3.27}$$

$$\mathrm{i}\dot{\boldsymbol{\varphi}} = (1-\mathrm{P})\boldsymbol{\rho}^{-1}\left\langle \mathrm{H}\right\rangle \boldsymbol{\varphi} + \mathrm{P}\boldsymbol{g}\mathbf{1}\boldsymbol{\varphi}. \tag{3.28}$$

3.1.4 The Mean Field Operator

While simple in appearance, there is a part of equations (3.27) and (3.28) that warrants a closer look; this part is the mean field operator $\langle \mathrm{H}\rangle$. When attempting to solve (3.27) and (3.28) it is the computaion of $\langle \mathrm{H}\rangle$ that will require the bulk of the work. Here we will examine the $\langle H\rangle_{kl}$ terms.

We first break $\langle H\rangle_{kl}$ up in terms of its one-body, $H_1(\boldsymbol{x}_i;t)$, and two-body, $H_2(\boldsymbol{x}_i,\boldsymbol{x}_j)$, operators. Using definitions (3.8) and (3.10) we get,

$$\begin{aligned}
\langle H\rangle_{kl} &= \sum_{i=1}^{f}\left\langle \Psi^{(k)}\middle|H_1(\boldsymbol{x}_i;t)\middle|\Psi^{(l)}\right\rangle + \sum_{j>i}^{f}\left\langle \Psi^{(k)}\middle|H_2(\boldsymbol{x}_i,\boldsymbol{x}_j)\middle|\Psi^{(l)}\right\rangle \\
&= \sum_{i=1}^{f}\sum_{j_2\ldots j_f}\sum_{l_2\ldots l_f} A^{*}_{kj_2\ldots j_f} A_{ll_2\ldots l_f}\left\langle \varphi_{j_2}\ldots\varphi_{j_f}\middle|H_1(\boldsymbol{x}_i;t)\middle|\varphi_{l_2}\ldots\varphi_{l_f}\right\rangle \\
&\quad + \sum_{j>i}^{f}\sum_{j_2\ldots j_f}\sum_{l_2\ldots l_f} A^{*}_{kj_2\ldots j_f} A_{ll_2\ldots l_f}\left\langle \varphi_{j_2}\ldots\varphi_{j_f}\middle|H_2(\boldsymbol{x}_i,\boldsymbol{x}_j)\middle|\varphi_{l_2}\ldots\varphi_{l_f}\right\rangle .
\end{aligned} \tag{3.29}$$

We will first examine the one-body part of equation (3.29) and look at the $i=1$ and $i\geq 2$ sepatately. For $i=1$ we have,

$$\begin{aligned}
&\sum_{j_2\ldots j_f}\sum_{l_2\ldots l_f} A^{*}_{kj_2\ldots j_f} A_{ll_2\ldots l_f}\left\langle \varphi_{j_2}\ldots\varphi_{j_f}\middle|H_1(\boldsymbol{x}_1;t)\middle|\varphi_{l_2}\ldots\varphi_{l_f}\right\rangle \\
&= \sum_{j_2\ldots j_f} A^{*}_{kj_2\ldots j_f} A_{lj_2\ldots j_f} H_1(\boldsymbol{x}_1;t) \\
&= \rho_{kl} H_1(\boldsymbol{x}_i;t)
\end{aligned} \tag{3.30}$$

and upon using (3.3) and rearranging the multi-indices to get $(f-1)$ equal terms, for $i\geq 2$ we get,

$$\begin{aligned}
&\sum_{i=2}^{f}\sum_{j_2\ldots j_f}\sum_{l_2\ldots l_f} A^{*}_{kj_2\ldots j_f} A_{ll_2\ldots l_f}\left\langle \varphi_{j_2}\ldots\varphi_{j_f}\middle|H_1(\boldsymbol{x}_i;t)\middle|\varphi_{l_2}\ldots\varphi_{l_f}\right\rangle \\
&= (f-1)\sum_{j_2,l_2}\sum_{j_3\ldots j_f} A^{*}_{kj_2j_3\ldots j_f} A_{ll_2j_3\ldots j_f}\left\langle \varphi_{j_2}\middle|H_1(\boldsymbol{x}_2;t)\middle|\varphi_{l_2}\right\rangle .
\end{aligned} \tag{3.31}$$

Similarly, for the two-body part we separate for $i=1$, $j=2$ to get,

$$\begin{aligned}
&\sum_{j_2\ldots j_f}\sum_{l_2\ldots l_f} A^{*}_{kj_2\ldots j_f} A_{ll_2\ldots l_f}\left\langle \varphi_{j_2}\ldots\varphi_{j_f}\middle|H_2(\boldsymbol{x}_1,\boldsymbol{x}_2)\middle|\varphi_{l_2}\ldots\varphi_{l_f}\right\rangle \\
&= (f-1)\sum_{j_2,l_2}\sum_{j_3\ldots j_f} A^{*}_{kj_2j_3\ldots j_f} A_{ll_2j_3\ldots j_f}\left\langle \varphi_{j_2}\middle|H_2(\boldsymbol{x}_1,\boldsymbol{x}_2)\middle|\varphi_{l_2}\right\rangle
\end{aligned} \tag{3.32}$$

and for $i \geq 2$, $j > i$ to get,

$$\sum_{i=2}^{f}\sum_{j=i+1}^{f}\sum_{j_2\ldots j_f}\sum_{l_2\ldots l_f} A^*_{kj_2\ldots j_f} A_{ll_2\ldots l_f} \left\langle \varphi_{j_2}\ldots\varphi_{j_f}\middle|H_2(\boldsymbol{x}_i,\boldsymbol{x}_j)\middle|\varphi_{l_2}\ldots\varphi_{l_f}\right\rangle$$
$$= \frac{(f-1)(f-2)}{2}\sum_{j_2,l_2}\sum_{j_3,l_3}\sum_{j_4\ldots j_f} A^*_{kj_2j_3j_4\ldots j_f} A_{ll_2l_3j_4\ldots j_f} \left\langle \varphi_{j_2}\varphi_{j_3}\middle|H_2(\boldsymbol{x}_1,\boldsymbol{x}_2)\middle|\varphi_{l_2}\varphi_{l_3}\right\rangle . \quad (3.33)$$

Where again we have used (3.3) and rearranged the multi-indices.

Looking at equations (3.31) and (3.33) we can see that these are not complex functions but merely complex numbers. Thus, when taking into consideration $1-P$, which projects onto the space orthogonal to the φ_i's, it is easy to see that these terms will disappear. The components of the mean field operator can now be written as,

$$\langle H\rangle_{kl} = \rho_{kl}H_1(\boldsymbol{x}_i;t) + (f-1)\sum_{j_2,l_2}\sum_{j_3\ldots j_f} A^*_{kj_2j_3\ldots j_f} A_{ll_2j_3\ldots j_f} \left\langle \varphi_{j_2}\middle|H_2(\boldsymbol{x}_1,\boldsymbol{x}_2)\middle|\varphi_{l_2}\right\rangle . \quad (3.34)$$

It is the evaluation of the $\langle\varphi_{j_2}|H_2(\boldsymbol{x}_1,\boldsymbol{x}_2)|\varphi_{l_2}\rangle$ terms and the summations in (3.34) that will require a significant amount of work. The calculation of these terms will be discussed in the next chapter.

3.1.5 Choice of constraints

Up to this point we have left the choice of the operator $g(t)$ in constraint (3.7), open. The only requirements were that $g(t)$ be a one-body, Hermitian operator. Here we will specify what choices of $g(t)$ will be used in our calculations.

The simplest choice is to use $g = 0$. Putting this into equations (3.27) and (3.28) yields,

$$\mathrm{i}\dot{A}_{j_1\ldots j_f} = \sum_{l_1\ldots l_f} A_{l_1\ldots l_f}\left\langle\varphi_{j_1}\ldots\varphi_{j_f}\middle|H\middle|\varphi_{l_1}\ldots\varphi_{l_f}\right\rangle \quad (3.35)$$

$$\mathrm{i}\dot{\boldsymbol{\varphi}} = (1-\mathrm{P})\boldsymbol{\rho}^{-1}\langle\mathrm{H}\rangle\boldsymbol{\varphi}. \quad (3.36)$$

It is this choice for g that will be implemented when using MCTDHF to find the bound state of a system. Another choice is $g = H_1$. Putting this into equations (3.27) and (3.28) gives,

$$\mathrm{i}\dot{A}_{j_1\ldots j_f} = \sum_{l_1\ldots l_f} A_{l_1\ldots l_f}\left\langle\varphi_{j_1}\ldots\varphi_{j_f}\middle|H_2\middle|\varphi_{l_1}\ldots\varphi_{l_f}\right\rangle \quad (3.37)$$

$$\mathrm{i}\dot{\boldsymbol{\varphi}} = \mathrm{H}_1\mathbf{1}\boldsymbol{\varphi} + (1-\mathrm{P})\boldsymbol{\rho}^{-1}\langle\mathrm{H}\rangle^{(2)}\boldsymbol{\varphi} \quad (3.38)$$

where $\langle\mathrm{H}\rangle^{(2)}$ is the two-body contribution of the mean field operator.

When examining the equations of motion for both $g = 0$ and $g = H_1$ there are a few things to note. First, the evolution of the spin-orbitals is less restricted in equation (3.38) than in equation (3.36). This is a result of the projector only acting on the interaction part in equation (3.36). Furthermore, as $n \to \infty$, that is, when the φ_j's form a conplete basis, the $1-\mathrm{P}$ term vanishes. Thus, in equation (3.38), even with a complete basis, the φ_j's continue to evolve with time, whereas, in equation (3.36) they remain static. Also, for $g = H_1$ the motion of the expansion coefficients is solely a result of electron correlation; however, when $g = 0$ it is the full Hamiltonian that causes the resulting motion.

Chapter 4

The MCTDHF program

In chapter 3 we introduced the MCTDHF method and derived a set of non-linear equations of motion that can be used to solve the TDSE. In this chapter we focus on how we actually solve these equations. To do this we have written a progam in the C programming language. Here we will present this program and discuss the details of how the calculations are performed. We will discuss how our grid is set up and how differentiation and integration are handled by the code. We will then discuss how we calculate the one and two electron terms on the right hand side (RHS) of equations (3.28) and (3.27). Finally, we will discuss how the MCTDHF wave function is propagated in time. For the purpose of this discuss we will write the $\varphi_j(\boldsymbol{q};t)$ in terms of its spatial and spin parts as $\varphi_j(\boldsymbol{q};t) = \varphi_j(\boldsymbol{x};t) \otimes s_j$.

4.1 The multi-electron Hamiltonian

Before we begin discussing how to solve the MCDTHF equations of motion we will first explicitly show the form of our Hamiltonian. Up until now we have presented the multi-electron hamiltonitan as $H = \sum_{i=1}^{f} H_1(\boldsymbol{x}_i;t) + \sum_{i<j}^{f} H_2(\boldsymbol{x}_i,\boldsymbol{x}_j)$ without explicitly stating the forms of H_1 and H_2. We write the single electron Hamiltonian in velocity gauge as,

$$H_1(\boldsymbol{x};t) = \frac{1}{2}(-\mathrm{i}\vec{\nabla} - \vec{A}(t))^2 + U(\boldsymbol{x}) \tag{4.1}$$

and the two-electron Hamiltonian as,

$$H_2(\boldsymbol{x}_1,\boldsymbol{x}_2) = \frac{1}{|\vec{\boldsymbol{x}}_2 - \vec{\boldsymbol{x}}_1|} \tag{4.2}$$

where $\vec{A}(t)$ is the vector potential of the laser electric field and $U(\boldsymbol{x})$ is some scalar potential.

4.2 The MCTDHF_User data type

When solving the MCTDHF equations most of the subroutines require many arguments to perform their specific calcuation. In order to avoid this we have created the **MCTDHF_User** data type. The **MCTDHF_User** data type is declared in the following way:

```
typedef struct {
    pointer p;
} MCTDHF_User;
```

where we have the **pointer** type is declared as:

```
typedef void* pointer;
```

This allows for any data type that we wish to create to be declared with type **MCTDHF_User**. In our program we create a structure called **RHS**; this has the form,

```
struct RHS {
   ⋮
}
```

and contains all the necessary variables and pointers that are needed to calculate the RHS of the MCTDHF equations. In the code we set up the **MCTDHF_User** type by the following lines:

```
struct RHS rhs;
MCTDHF_User comm;
comm.p = (pointer)&rhs;
```

When passed into a subroutine of the form F(...,MCTDHF_User *comm) the data stored in **comm** can be accessed in the following way:

(i) **struct** RHS *s = (**struct** RHS*)comm->p;
(ii) s->a, where a is a variable or pointer in **comm**

4.3 Differentiation and Integration

The grid used to solve the MCTDHF equations is specified by choosing the number of dimensions for the calculation and then specifying s maximum value and the number of points to be used for each axis (the code allows for a different number of points and a different range for each coordinate axis). A uniform grid spacing is used along each coordinate axis. For each axis the grid spacing and grid points are determined by:

$$\Delta x = \frac{2x_{max}}{N} \tag{4.3}$$

$$x_j = -x_{xmax} + j\Delta x \tag{4.4}$$

where x_{max} is the maximum value for the coordinate axis and N is the number of points. The corresponding grid in momentum space is then determined by:

$$\Delta k = \frac{\pi}{x_{max}} \tag{4.5}$$

$$k_j = j\Delta k. \tag{4.6}$$

In order to compute $H_1(\boldsymbol{x};t)\varphi_j(\boldsymbol{x};t)$ we need to calculate the terms $\nabla\varphi_j(\boldsymbol{x};t)$ and $\nabla^2\varphi_j(\boldsymbol{x};t)$. These are done in the code by:

$$\mathrm{i}\nabla\varphi_j(\boldsymbol{x};t) = -F^{-1}[\hat{k}\tilde{\varphi}_j(\boldsymbol{k};t)] \tag{4.7}$$

$$-\nabla^2\varphi_j(\boldsymbol{x};t) = F^{-1}[\hat{k}^2\tilde{\varphi}_j(\boldsymbol{k};t)] \tag{4.8}$$

where F^{-1} is the inverse Fourier transform. At first this may appear to be a less efficient way to compute the partial derivatives than using finite difference. However, as we shall see, we will need to take the Fourier transforms of the φ_j's anyway when calculating the mean field. In the code the Fourier transforms are computed using FFTW, an efficient program for computing fast Fourier transforms (FFT) [1].

The code performs integration of a function $f(x)$, along a coordinate axis, using the trapezoidal rule [61]. For the above described space discretization we have,

$$\int_{x_i}^{x_{i+1}} f(x)dx \approx \frac{\Delta x}{2}[f(x_{i+1}) + f(x_i)]. \tag{4.9}$$

4.4 The equations of motion and initial conditions

Before we begin discussing how we calculate the RHS's of equations (3.27) and (3.28), we will rewrite them in a way that allows us to get a clearer view of what we need to calculate. We will set the constraint operator to be $g = 0$ as this will allow us to cover all aspects of the calculation[2]. First we define the following terms:

$$H^{(1)}_{mk} := \langle\varphi_m|H_1|\varphi_k\rangle\,\delta_{s_m s_k} \tag{4.10}$$

$$H^{(2)}_{jklm} := \langle\varphi_j\varphi_k|H_2|\varphi_l\varphi_m\rangle\,\delta_{s_j s_l}\delta_{s_k s_m} \tag{4.11}$$

$$\Phi_{k\pm}(\boldsymbol{x};t) := \sum_{jl}(\rho^{-1})_{kj}\,\langle H\rangle^{(2)}_{jl}\,\delta_{s_l\pm}\varphi_l(\boldsymbol{x};t) \tag{4.12}$$

and then rewrite equation (3.27) as,

$$\begin{aligned}
\mathrm{i}\dot{A}_{j_1\ldots j_f} = &\sum_k[H^{(1)}_{j_1k}A_{kj_2\ldots j_f} + H^{(1)}_{j_2k}A_{j_1kj_3\ldots j_f} + \ldots + H^{(1)}_{j_fk}A_{j_1\ldots j_{f-1}j_k}|\\
&+\sum_{kl}[H^{(2)}_{j_1j_2kl}A_{klj_3\ldots j_f} + H^{(2)}_{j_1j_3kl}A_{kj_2lj_4\ldots j_f}\ldots + H^{(2)}_{j_1j_fkl}A_{kj_2\ldots j_{f-1}l}\\
&+H^{(2)}_{j_2j_3kl}A_{j_1klj_4\ldots j_f} + \ldots + H^{(2)}_{j_2j_fkl}A_{j_1kj_3\ldots j_{f-1}l} + \ldots\\
&+H^{(2)}_{j_{f-1}j_fkl}A_{j_1\ldots j_{f-2}kl}]
\end{aligned} \tag{4.13}$$

and equation (3.28) as,

$$\begin{aligned}
\mathrm{i}\dot{\varphi}_k(\boldsymbol{x};t)\otimes s_k = &H_1(\boldsymbol{x};t)\varphi_k(\boldsymbol{x};t)\otimes s_k - \sum_m H^{(1)}_{mk}\varphi_m(\boldsymbol{x};t)\otimes s_m + \Phi_{k+}(\boldsymbol{x};t)\otimes s_{+\frac{1}{2}}\\
&+\Phi_{k-}(\boldsymbol{x};t)\otimes s_{-\frac{1}{2}} - \sum_m \delta_{s_m+}\,\langle\varphi_m|\Phi_{k+}\rangle\,\varphi_m(\boldsymbol{x};t)\otimes s_m\\
&-\sum_m \delta_{s_m-}\,\langle\varphi_m|\Phi_{k-}\rangle\,\varphi_m(\boldsymbol{x};t)\otimes s_m.
\end{aligned} \tag{4.14}$$

[1] www.fftw.org

[2] As we shall see using when $g = H_1$ we will not be required to calculate the $\langle\varphi_i|H|\varphi_j\rangle\,\delta_{s_i s_j}$ terms.

To solve the above system we need only specify some initial conditions and then propagate equations (4.13) and (4.14) in time. The code currently sets up the initial spin-orbital functions in the following manner:

$$\begin{aligned}
\varphi_1(\boldsymbol{x};0)\otimes s_1 &= \varphi_1(\boldsymbol{x};t)\otimes s_{+\frac{1}{2}}\\
\varphi_2(\boldsymbol{x};0)\otimes s_2 &= \varphi_1(\boldsymbol{x};t)\otimes s_{-\frac{1}{2}}\\
&\vdots\\
\varphi_{n-1}(\boldsymbol{x};0)\otimes s_{n-1} &= \varphi_{n-1}(\boldsymbol{x};t)\otimes s_{+\frac{1}{2}}\\
\varphi_n(\boldsymbol{x};0)\otimes s_n &= \varphi_{n-1}(\boldsymbol{x};t)\otimes s_{-\frac{1}{2}}
\end{aligned}$$

That is, every second spin orbital function starts with the same spatial part as the one before it but with opposite spin. The code chooses the intial spatial parts to be the bound states of the harmonic oscillator [62]; we choose these initial states because they already form an orthonormal basis. However, the code is written in such a way that any set of linearly independent spin orbital functions can be used initially; the code will orthonormalize the basis prior to beginning propagation. The $A_{j_1\ldots j_f}$ coefficients are set to $[\binom{n}{f}f!]^{-\frac{1}{2}}$ which, along with the orthonormal basis, will ensure the initial wave function is normalized.

4.5 Indexing and summation

When writing the MCTDHF code in a general way, so that the user can specify any number of electrons and any number of spin-orbital functions to be used in his/her caluclation, a major challenge that presented itself was how to deal with indexing the $A_{j_1\ldots j_f}$ coefficients and how to perform the multi-index summations that appear in the mean-field and the density matrix. Since the number of indices in the A coefficients is dependent on the number of electrons, f, we needed to write the code so that summation over sets of A coefficients, as in (3.34), can be done without have large amounts of nested loops. To do this the $A_{j_1\ldots j_f}$ are stored such that $j_1 < j_2 < \ldots < j_f$. That is, we store only the $\binom{n}{f}$ independent $A_{j_1\ldots j_f}$'s and then use equation (3.3) to access the coefficients that don't have indices ordered as above.

The A coefficients are stored in an array of length $\binom{n}{f}$ such that the first element contains the $A_{j_1\ldots j_f}$ value corresponding to the set of ordered indices that sum to the smallest number, the second elements has the set of indices that sum to the second lowest number etc. For example, if we had f = 3 and n = 5 then the array holding the A coefficients would be $A[0] = A_{123}$, $A[1] = A_{124}$, $A[2] = A_{125}$, $A[3] = A_{134}$, $\ldots$, $A[9] = A_{345}$ [3]. Given a set $\{j_1 \ldots j_f : j_i \neq j_k \forall i,\, k\}$ (the j_i's need not be ordered) the index corresponding to $A_{j_1\ldots j_f}$ in the A array is found by the function **getindex**. This function has the prototype:

int getindex(**int** *a, **int** f, **int** n, **int** **C).

Here the pointer **a** contains the values $a[0] = j_1, \ldots, a[f-1] = j_f$ and **C** is a double pointer such that $C[m][k] = \binom{m}{k}$. So using our example above, with $f = 3$ and $n = 5$, if $a = [2, 3, 5]$ the **getindex** would return the value 7.

[3] In the code the A coefficients are not held in an array A, but at the end of the array *psi* that holds the spin-orbital functions. The array A here is used merely to clarify the how the indexing is done.

In equations (3.9) and (3.34) there are summations over many indices. In order to do these summations we rewrite (3.9) as,

$$\rho_{kl} = (f-1)! \sum_{j_2<\ldots<j_f} A^*_{kj_2\ldots j_f} A_{lj_2\ldots j_f} \tag{4.15}$$

and, in a similar manner, we rewrite the two-body part of (3.34) as,

$$\langle H\rangle^{(2)}_{jl} = (f-1)! \sum_{j_2,l_2} \langle\varphi_{j_2}|H_2|\varphi_{l_2}\rangle \sum_{j_3<\ldots<j_f} A^*_{jj_2j_3\ldots j_f} A_{ll_2j_3\ldots j_f}. \tag{4.16}$$

In order to get the density matrix we use the subroutine **getrho**. This subroutine has the prototype:

void getrho(fftw_complex *A, MCTDHF_User *comm)

For each set $\{k,l\}$ the element ρ_{kl} is calulated by **getrho** in the following way:

(i) A variable **size** to be $n-1$ if $k=l$ and $n-2$ otherwise.
(ii) An array **js** is set up to have length **size**.
(iii) The smallest remaining possible index values are placed, in order, in **js**; that is, the arrangement is such that $js[0] < js[1] < \ldots$ etc.
(iv) Sets the variable **nrows** to be $nrows = \binom{size}{f-1}$
(v) A matrix **B**, of size $nrows \times (f-1)$, is set up. This contains all ordered combinations of index values form the set $\{j_i : i = 1\ldots n,\ j_i \neq k,l\}$.
(vi) For each "row", i, of B we create the array **indc** $= [k, B[i][0], \ldots, B[i][f-2]]$ and the array **ind** $= [l, B[i][0], \ldots, B[i][f-2]]$.
(vii) **ind** and **indc** are passed to the subroutine **getsign** to determine if they are a positive or negative permution of the coefficient we have stored.
(viii) The index for **ind** and **indc** are determined using **getindex**.
(ix) The value of $A^*_{kj_2\ldots j_f} A_{lj_2\ldots j_f}$ is then calculated and added to the sum.
(x) Once the summation is complete we multiply by $(f-1)!$.

The summation over $j_3 \ldots j_f$ in equation (4.16) is done using the subroutine **getAsum**. This does the summation in a similar way as discribed above. The main difference being that we have four indices, j, j_2, l and l_2 that remain constant. The variable **size** is then set to $n-4$ if none of the j, j_2, l and l_2 are equal; $n-3$ if one, and only one, of $j=l$, or $j=l_2$, or $j_2=l$ or $j_2=l_2$ occurs; and $n-2$ if one of $j=1$ and $j_2=l_2$ or $j=l_2$ and $j_2=l$ occurs. When three or four of the j, j_2, l and l_2 are equal we do not get a contribution to the sum. The function prototype for **getAsum** is:

void getAsum(**int** f,**int** n,**int** j,**int** l,**int** j2,**int** l2,fftw_complex *A,**int** **C, fftw_complex Asum)

4.6 The one-body operator

The first terms in equation 4.13 and the first two terms in equation 4.14 involve the one-body operator H_1. In velocity gauge the action of H_1 on φ_j is calculated using (4.7) and (4.8) by,

$$H_1(\boldsymbol{x};t)\varphi_j(\boldsymbol{x};t) = F^{-1}[(\frac{1}{2}\hat{k}^2 - \hat{k}\cdot A(t))\tilde{\varphi}_j(\boldsymbol{k};t)] + [U(\boldsymbol{x}) + \frac{1}{2}A(t)^2]\varphi_j(\boldsymbol{x};t) \tag{4.17}$$

and in length gauge, using (4.8), as

$$H_1(\boldsymbol{x};t)\varphi_j(\boldsymbol{x};t) = \frac{1}{2}F^{-1}[\hat{k}^2\tilde{\varphi}_j(\boldsymbol{k};t)] + [U(\boldsymbol{x}) + \hat{\boldsymbol{x}}\cdot E(t)]\varphi_j(\boldsymbol{x};t) \tag{4.18}$$

The TDSE is transformed from length gauge to velocity gauge using the unitary transformation:

$$\Psi_l(\vec{x};t) = e^{-i\vec{A}(t)\cdot\vec{x}}\Psi_v(\vec{x};t) \tag{4.19}$$

$$\vec{A}(t) = \int_t^\infty \vec{E}(t')dt' \tag{4.20}$$

Where, Ψ_l and Ψ_v represent the wave function in the length and velocity gauges respectively. The matrix elements in definition (4.10) are calculated as,

$$H^{(1)}_{jk} = \delta_{s_j s_k}\int d\boldsymbol{x}\varphi^*_j(\boldsymbol{x};t)[H_1(\boldsymbol{x};t)\varphi_j(\boldsymbol{x};t)] \tag{4.21}$$

The code only calculates $H^{(1)}_{jk}$ for $k > j$ and then uses the relation $H^{(1)}_{jk} = (H^{(1)}_{kj})^*$. In the code these calcuations are done by the subroutine **getH1mat**; this has the prototype:

void getH1mat fftw_complex *psi, fftw_complex *phir, MCTDHF_User *comm)

getH1mat calculates the $H^{(1)}_{jk}$ terms and the action of H_1 on the spin-orbital basis in the following way:

(i) Calculate $\mathbf{A}$(t) (or $\mathbf{E}$(t) in length gauge).
(ii) Loop through j and calculate $H_1\varphi_k$ using (4.17) or (4.18)
(iii) Loop through $k \geq j$. If $s_k = s_j$ calculate $H^{(1)}_{jk}$ from (4.21); otherwise set $H^{(1)}_{jk} = 0$.
(iv) Set $H^{(1)}_{kj} = (H^{(1)}_{jk})^*$.

4.7 The mean-field

In order to calculate the mean field we must calculate the $\langle\varphi_i|H_2|\varphi_j\rangle$ terms; we will label these term as V_{ij}. From (4.2) we can write $H_2(\boldsymbol{x}_1,\boldsymbol{x}_2) = H_2(\boldsymbol{x}_2 - \boldsymbol{x}_1)$ and letting $f_{ij}(\boldsymbol{x}) = \varphi^*_i(\boldsymbol{x};t)\varphi_j(\boldsymbol{x};t)$ we must evalute the integral

$$V_{ij}(\boldsymbol{x}_2) = \int d\boldsymbol{x}_1 f_{ij}(\boldsymbol{x}_1)H_2(\boldsymbol{x}_2 - \boldsymbol{x}_1) \tag{4.22}$$

to obtain the V_{ij} terms. Since $V_{ij} = V^*_{ji}$ we have $n+\binom{n}{2}$ independent V_{ij} terms. If we have N mesh points, then computation of each V_{ij} term will require approximately N^2 operations. Thus, in order to obtain all of the independent V_{ij} terms we are looking at $\sim N^2[n + \binom{n}{2}]$ operations. For example, if we were doing a two-dimensional calculation on a 512×128 grid (ie: $N = 65536$) with 10 spin-orbital basis functions then we would require $\sim 2.4 \times 10^{11}$ operations to obtain all independent V_{ij}'s by straight evaluation of the integral in equation (4.22).

In order to compute the integral in equation (4.22) we note that this is just a convolution integral. Thus using the *convolution theorem* [63] we calculate the V_{ij} terms by,

$$V_{ij}(\boldsymbol{x}) = F^{-1}[\tilde{f}_{ij}(\boldsymbol{k})\tilde{H}_2(\boldsymbol{k})]. \tag{4.23}$$

In the code, $\tilde{H}_2$ is calculated at the beginning by,

$$\tilde{H}_2(\boldsymbol{k}) = F\left[\frac{1}{\sqrt{\boldsymbol{x}\cdot\boldsymbol{x}+a^2}}\right] \tag{4.24}$$

and the results are stored in the array **Veek**; a is a shielding parameter. Thus, in order to calculate the V_{ij} terms using equation (4.23) we need to do the following:

(i) Calculate $F[f_{ij}(\boldsymbol{x})]$
(ii) Multiply $\tilde{f}_{ij}(\boldsymbol{k})$ by $\tilde{H}_2(\boldsymbol{k})$
(iii) Calculate the inverse transform of $\tilde{f}_{ij}(\boldsymbol{k})\tilde{H}_2(\boldsymbol{k})$

The Fourier transforms are done by FFT routines and thus scale as $N\log_2 N$. Hence, calculating the V_{ij} terms using (4.23) requires $\sim 2N\log_2 N[n+\binom{n}{2}]$ operations. In the case of our example above, this would work out to $\sim 1.15\times 10^8$ operations. That is, evaluation of V_{ij} by (4.22) would require approximately 2000 times more computational work than using (4.23). The V_{ij} are calculated in the code by the subroutine **getVmat**. This has the function prototype:

void getVmat(fftw_complex *y, MCTDHF_User *comm).

To calculate the two-electron part of the mean-field operator, $\langle H\rangle^{(2)}$, the subroutine **getMFH2** is used. This function has the prototype:

void getMFH2(fftw_complex *y, MCTDHF_User *comm).

It calculates $\langle H\rangle^{(2)}_{jl}$, using equation (4.16), by looping through j_2 and l_2 and doing the following:

(i) $\sum_{j_3<\ldots<j_f} A^*_{jj_2j_3\ldots j_f}A_{ll_2j_3\ldots j_f} \rightarrow$ **Asum**
(ii) Multiplying **Asum** by $V^*_{j_2l_2}$ if $j_2 > l_2$ and by $V_{j_2l_2}$ otherwise
(iii) Setting $\langle H\rangle^{(2)}_{jl} + \textbf{Asum}V_{j_2l_2} \rightarrow \langle H\rangle^{(2)}_{jl}$

Once we have looped through all j_2's and l_2's we multiply $\langle H\rangle^{(2)}_{jl}$ by $(f-1)!$. This is then repeated for the next set of j and l.

To calculate the $H^{(2)}_{jklm}$ terms we use the subroutine **getH2mat**. This has the protoype:

void getH2mat(fftw_complex *y, MCTDHF_User *comm).

In order to calculate the H_{jklm} terms more efficiently, this subroutine makes use of the relation:

$$H^{(2)}_{jklm} = H^{(2)}_{kjml}. \tag{4.25}$$

Using relation (4.25) in a calulation with n spin-orbital functions, we need only calculate $n[n+\binom{n}{2}] + n^2\binom{n}{2} = \frac{n^2}{2}[n^2+1]$ of the $H^{(2)}_{jklm}$ terms. If we did not make use of this we would be required to calculate n^4 terms. So, for example, if $n = 10$ we need only calculate 5050 terms as opposed to 10^4 terms; this is roughly half the amount of calculation. **getH2mat** calculates the $H^{(2)}_{jklm}$ terms by looping through $j = 1\rightarrow n$, $k = j\rightarrow n$ and $m = 1\rightarrow n$. Each H_{jklm} term is then calculated in the following way:

(i) If $s_k = s_l$ then calculate $\varphi^*_j V_{km}$; otherwise loop through l and set $H^{(2)}_{jklm} = H^{(2)}_{kjml} = 0$.
(ii) Loop through l. If $s_k = s_l$ and $s_j = s_m$ then calculate $H^{(2)}_{jklm} = \int dx(\varphi^*_j V_{km})\varphi_l$; otherwise set $H^{(2)}_{jklm} = 0$.
(iii) Set $H^{(2)}_{kjml} = H^{(2)}_{jklm}$.

4.8 Summations in the time derivative of the A coefficients

The summation for the first part of the RHS of equation (4.13) is done by the subroutine **getH1sum**. This has the function prototype:

void getH1sum(fftw_complex *A, MCTDHF_User *comm, int *js, fftw_complex H1sum).

Here the pointer **js** is the set of j_i's that appear in the left hand side (LHS) of equation (4.13). **getH1sum** calculates the summation by setting **H1sum** equal to zero and then looping through $k = 1 \rightarrow n$ and using an index $l = 1 \rightarrow f$ to reference the place in the $j_1 \ldots j_f$ that k replaces. We then search through the j_i's. If $j_i = k$ and $i \neq l$ we break from the loop and increase l; otherwise we add each term to the sum in the following way:

(i) Set up a pointer called **js2**. This is the same as **js** but with $js2[l] = k$.
(ii) Call **getsign** to get the sign of the permutation; this variable is called **sign**.
(iii) Call **getindex** to determine the index for the A coefficient; this is stored in **index**.
(iv) Multiply $sign \times A[index] \rightarrow$ **temp**
(v) **H1sum** + $H^{(2)}_{j_l k} \times temp \rightarrow$ **H1sum**

The summation in the second part of the RHS of equation (4.13) is done by the subroutine **getH2sum**. This has the prototype:

void getH2sum(fftw_complex *A, MCTDHF_User *comm, int *js, fftw_complex H2sum)

getH2sum works in a similar way to **getH1sum** except that this time we need two place holder indices m and i such that $j_m = k$ and $j_i = l$. We begin by looping through $m = 0 \rightarrow f - 2$, $k = 1 \rightarrow n$, $i = m + 1 \rightarrow f - 1$ and $l = 1 \rightarrow n$. For $l \neq k$, as in **getH1sum**, we set up a pointer labeled **js2**. Again, this is the same as **js** except we set $js2[m] = k$ and $js2[i] = l$. For $l \neq k$ we add each term to the sum in the following way:

(i) For $l \neq k$ set up a pointer labeled **js2**. Again, this is the same as **js** except we set $js2[m] = k$ and $js2[i] = l$.
(ii) If $f > 2$ check to make sure none of the j_i are equal to k or l.
(iii) Call **getsign** to get the sign of the permutation and store it in **sign**.
(iv) Call **getindex** to determine the index for the A coefficient; this is stored in **index**.
(v) Multiply $sign \times A[index] \rightarrow$ **temp**
(vi) **H1sum** + $H^{(2)}_{j_m j_i k l} \times temp \rightarrow$ **H1sum**

4.9 Time propagation

Time propagation in the MCTDHF program is done in the momentum domain using a fourth-order Runge-Kutta method. The code allows the calculation to be done in either length or velocity gauge; however, most of our calcuations are done in velocity gauge.

When finding the ground state of a system it has been shown that imaginary time propagation has better convergences properties [64]; this can be done by setting $t = -i\tau$. Our propagator then becomes $e^{-\mathrm{H}\tau}$ and thus we have the formal solution

$$|\Psi(\tau)\rangle = \alpha_0 e^{-E_0\tau}|\Psi_0\rangle + \alpha_1 e^{-E_1\tau}|\Psi_1\rangle + \ldots \tag{4.26}$$

where E_i and Ψ_i are the eigenvalues and eigenfunctions of the full Hamiltonian H [65]. Since E_0 is the smallest energy, as $\tau \rightarrow \infty$, $\Psi \rightarrow \Psi_0$ provided that Ψ is renormalized after each step. In the

MCTDHF code the spin-orbitals are orthonormalized using the Gram-Schmidt orthonormalization procedure after each time step. We then normalize Ψ by adjusting the expansion coefficients such that,

$$A_{j_1 \ldots j_f} \cdot \left[f! \sum_{j_1 < \ldots < j_f} |A_{j_1 \ldots j_f}|^2 \right]^{-\frac{1}{2}} \rightarrow A_{j_1 \ldots j_f} \tag{4.27}$$

When solving the MCTDHF equations of motion in imaginary time we set the constraint operator, g, to be $g = 0$. Starting from a bound state we then "turn on" the laser pulse and propagate the resulting wave function in real time. Here we have the choice of using $g = 0$ or $g = H_1$. While not yet fully tested, using $g = H_1$ has the advantage that it allows for the use of split-step [60] or composite Runge-Kutta [66] integration schemes.

Chapter 5

Ionization dynamics of N_2 in a strong laser field

In this chapter we first present some background information on laser matter interaction and then put the MCTDHF code to the test. The ionization dynamics of N_2 in the presence of a strong laser field will be investigated in two dimensions. We will present a simple classical model and compare its results with the results from our quantum mechanical calculations.

5.1 Laser field ionization of atoms and molecules

Many important phenomena occur when matter is in the presence of a strong laser field; some of these phenomena include above-threshold ionization (ATI) [67] and high harmonic generation (HHG) [68]. The key process causing these strong-field phenomena is ionization. When an atom or molecule is exposed to a stong-laser field its Coulomb potential is modified. This change can lower the Coulomb barrier and allow for ionization to occur.

Ionization can be characterized by the Keldysh parameter [69, 70] γ given by,

$$\gamma = \sqrt{\frac{I_p}{2U_p}} \tag{5.1}$$

where I_p is the ionization potential and U_p is the ponderomitive energy [71, 72]. U_p is the mean kinetic energy gained by an electron in an ocsillating electric field of strength E and frequency ω; U_p is given by,

$$U_p = \frac{E^2}{4\omega^2} \tag{5.2}$$

For γ there are essentially two parameter ranges used to describe ionization. These ranges are defined by $\gamma \gg 1$ and $\gamma \ll 1$ and are discussed in the next section.

5.1.1 Ionization regimes

For $\gamma \gg 1$ matter is interacting with a field of moderate strength ($\approx 10^{13}\, W/cm^2$). In this range ionization is described by a multiphoton process. Here ionization occurs by the simultaneous absorption of N photons, where N is greater than or equal to the smallest number of photons required for an electron to reach the continuum. The excited electron can emit a lower wavelength photon and make a transition to a bound state (optical harmonic generation) [73] or it can become ionized and leave its parent nucleus (ATI).

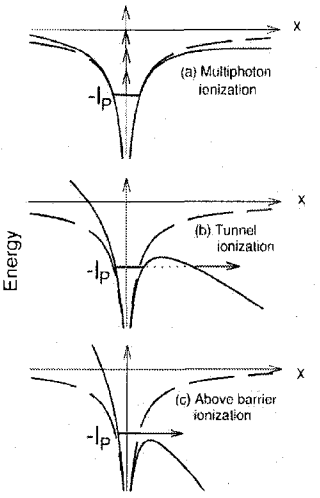

Figure 5.1. Different ionization prcesses. When an atom or molecule is exposed to an intense laser electric field the Coulomb potential (dashed curve) will be modified and result in a composition of the Coulomb barrier and the time-dependent external field (solid curve). (a) At moderate intensities the barrier has little suppression and ionization occurs through a multiphoton process. (b) At larger intensities the barrier becomes narrow and allows for electron wave function to penetrate the barrier. As a result the electron is tunnel ionized. (c) At extremely high intensities the Coulomb barrier is supressed below the bound state of the electron allowing for above barrier ionization. I_p is the ionization potential.

In the regime where $\gamma \ll 1$ the laser field significantly modifies the Coulomb potential. In this regime the dominant ionization process is tunnel ionization. With this type of ionization the Coulomb barrier is lowered enough that an electron's wave function penetrates the barrier and causes tunneling to occur; this happens within a fraction of the laser cycle [70, 74]. Tunneling ionization is best described by Ammosov-Delone-Krainov (ADK) theory [75] where tunnel ionization probabilites are determined unsing the quasistatic approximation. That is, ADK theory uses the fact that there is no significant change in the field during tunnel ionization.

A third type of ionization occurs when the field is strong enough to cause the supression of the Coulomb barrier to be greater than the ionization potential of an atom or molecule. The electron can then escape directly from the well without tunneling [76, 77]. This process is known as above barrier ionization (ABI). A schematic of these ionization processes can be seen in figure 5.1 [70].

5.1.2 The evolution of the electron in a laser field

Once the electron has been ionized it will experience an acceleration due to the presence of the laser-electric field. The motion of the electron in the field can be explained be a simple three-step model [67] depicted in figure 5.2[70]. When the laser field sufficiently supresses the Coulomb

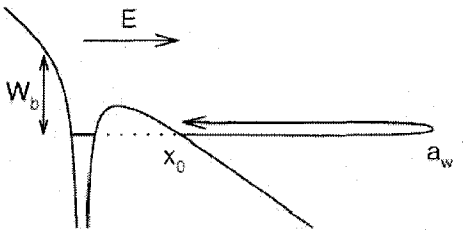

Figure 5.2. Schematic of the three step model for the evolution of an electron in an external lase field. W_b is the enegy of the most weakly bound electron and a_w is the maximum amplitude during the first excursion.

barrier the most weakly bound electron, with energy $-W_b$, can tunnel through the barrier and appear on the other side at position x_0. It is then accelerated in the laser field and returns to its parent ion within a fraction of a laser cycle.

This three-step model has proven very useful in providing a simple explanation of many strong field phenomena. For instance, it is useful for explaining the process of high-order harmonic generation (HHG) in a semiclassical way [68]. HHG occurs when high-order harmonic radiation, in the extreme ultraviolet (XUV) and soft-x-ray spectral range, is generated by the interaction of an intense linearly polarized laser field with atoms, atom clusters, and molecules. When the laser field lowers the Coulomb barrier an electron wave packet is set free at some time τ_b by tunnel ionization. It is then accelerated in the laser field where it aquires energy. Then approximately one cycle later the electron returns to the nucleus at some time τ. It then recombines to the ground state, with energy W_b and emits a high-energy photon by releasing the energy it gained in the field plus W_b. This process is illustrated in figure 5.3 [70]. HHG occurs most strongly for linearly polarized light. In the case of circularly polarized light the electron will completely miss its parent ion upon its return. A fully quantum mechanical theory of HHG for linearly polarized light can be seen in reference [72] and for elliptically polarized light in reference [78].

5.1.3 Nonsequential ionization

At sufficiently high laser intensities atoms and molecules can undergo multiple ionizations. Originally these multiple ionizations were thought to occur by the sequential stripping process where the atom is ionized, then the singly charged ion, then doubly charged ion, etc [76]. Experiments, however, showed that there also exists a nonsequential process that is responsible for multiple ionization [44, 79].

Several models for nosequential ionization have been proposed. In the *recollision model* [68], an atom or molecule is ionized by tunnel ionization. The ionized electron is then accelerated in the laser field and returns to the parent ion with considerable kinetic energy, after about half of an optical field cycle. The second electron is then emitted as a result of an inelastic scattering process. Another proposed mechanism is *shakeoff* [80]. Here there is a rapid change in the potential felt by the second electron due to the release of the first electron. That is, the second electron cannot adiabatically readjust to the ionic potential and is thus brought up into the continuum. A third mechanism, the *collective tunneling* mechanism [81], has also been proposed.

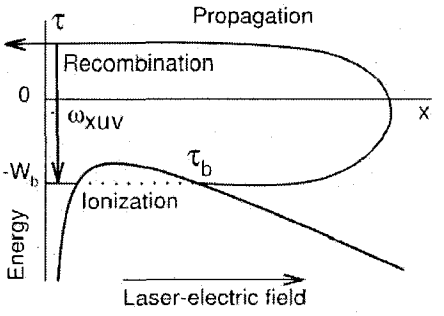

Figure 5.3. Illustration of the process involved in HHG. The electron is "born" outside the potential at time τ_b. It then accelerates in the laser field and returns at some later time τ. Upon recombining with the parent ion an high-energy XUV photon.

In this case both electrons simultaneously tunnel through the barrier and are ejected from the parent atom.

Both theoretical analysis [82] and experiment [83, 84, 85] have shown that recollision is the dominant process governing nonsequential ionization in the strong field regime. Nonsequential ionization caused by recollision of the ionized electron with its parent ion is known to occur in two ways - simultaneous emission or delayed tunnel ionization [86]. The momentum component of the ionized electrons parallel to the field polarization direction $k_{1,2}^{\parallel}$ is determined by their birth time in the electric field; the components perpendicular to the polarization direction $k_{1,2}^{\perp}$ will not be affected by the field in a significant way [87]. During simultaneous emission the two electrons leave the parent ion at the same time and thus will have similar momenta parallel to the field polarization direction. In the case of the delayed tunnel ionization the first electron excites the second during recollision. The second electron is then field ionized at some later time. Thus, for delayed tunnel ionization, $k_2^{\parallel}$ will differ from that of $k_1^{\parallel}$.

5.2 Strong field ionization of N_2 molecules

Over the last few years experiments have been performed using ensembles of aligned N_2 molecules. It was shown that single ionization was much more probable for molecules aligned parallel to the field direction than for those aligned perpendicular [88]. It was also shown that nonsequential double ionization (NDSI) depends on the orientation of the molecule [89]. For molecules aligned parallel to the laser field both electrons were more likely be emitted in the same direction during the same laser half cycle. When the molecule is aligned perpendicular to the field there is a time delay between emission of the two electrons and thus they are emitted during different half cycles. In addition it was observed that the average momentum of the escaping electrons was higher for molecules aligned parallel to field direction [89].

In our calculations we consider a 2-D N_2 molecule, in the presence of linearly polarized laser-electric field directed along the x-axis. The Coulomb potential, in the Born approximation,

is given by,

$$U(x,y) = -\frac{1}{\sqrt{(x-x_1)^2+(y-y_1)^2+b^2}} - \frac{1}{\sqrt{(x-x_2)^2+(y-y_2)^2+b^2}} \tag{5.3}$$

where $(x_{1,2}, y_{1,2})$ are the positions of the nitrogen atoms and b is a smoothing parameter. The atoms are centred at $(x_{1,2}, y_{1,2}) = (\pm 1.04, 0)$ [1] and the smoothing parameter is given by $b = 0.7129$. We use a two cycle pulse of wavelength $\lambda = 800$ nm and maximum field intensity $2 \times 10^{14}\ W/cm^2$. The vector potential of the pulse has a sine squared envelope with a period of 5.2 fs and is given by,

$$\vec{A}(t) = \frac{E_0}{\omega} \sin^2\left(\frac{\omega t}{4}\right) \sin(\omega t)\vec{k}_x \tag{5.4}$$

where E_0 is amplitude of the electric field and ω is the pulse frequency.

5.2.1 The classical model

In our classical model we examine the dynamics of the first ionized electron for different birth times (τ_b) in the laser-electric field. The electron is born in the field at a position $x_0 = x(\tau_b)$ and its motion in the field is governed by,

$$\ddot{x}(\tau) = -\vec{E}(\tau) \tag{5.5}$$

$$\dot{x}(\tau) = \vec{A}(\tau) - \vec{A}(\tau_b) + v_0 \tag{5.6}$$

where v_0 is an initial velocity, $\vec{A}$ is the vector potential, $\vec{E}$ is the electric field and $x(t)$ can be found from,

$$x(\tau) = \int_{\tau_b}^{\tau} \dot{x}(\tau)d\tau + x_0 \tag{5.7}$$

for electrons ionized from a bound state $v_0 = 0$. However, v_0 may not be zero for a recolliding electron after the collision; this depends on how much energy it loses during recollision. Due to the small molecular extension of N_2 we use $x_0 = 0$.

Since $A(\tau) = 0$ at the end of the pulse it is clear from equation (5.6) that the final drift momentum of the electron is completely determined by its birth time in the laser-electric field. The return time (τ_r) of the ionized electron is then determined as a function of the birth time by solving,

$$x(\tau_r) - x_0 = 0. \tag{5.8}$$

Once τ_r has been determined the velocity, and hence the energy, of the returning electron can be calculated. If the returning electron has enough energy to excite the bound electron to an excited state then the return electron will aquire a new drift velocity of

$$-A(\tau_r) + sgn(\dot{x}(\tau_r))\sqrt{2(E(\tau_r) - \Delta E)} \tag{5.9}$$

where $E(\tau_r)$ is the energy of the return electron at τ_r and ΔE is the energy difference between the ground and excited state. If, at any time τ_b' after τ_b, the barrier is suppressed below the

[1] This is for parallel alignment with the pulse. In the case of perpendiclar alignment we set $(x_{1,2}, y_{1,2}) = (0, \pm 1.04)$.

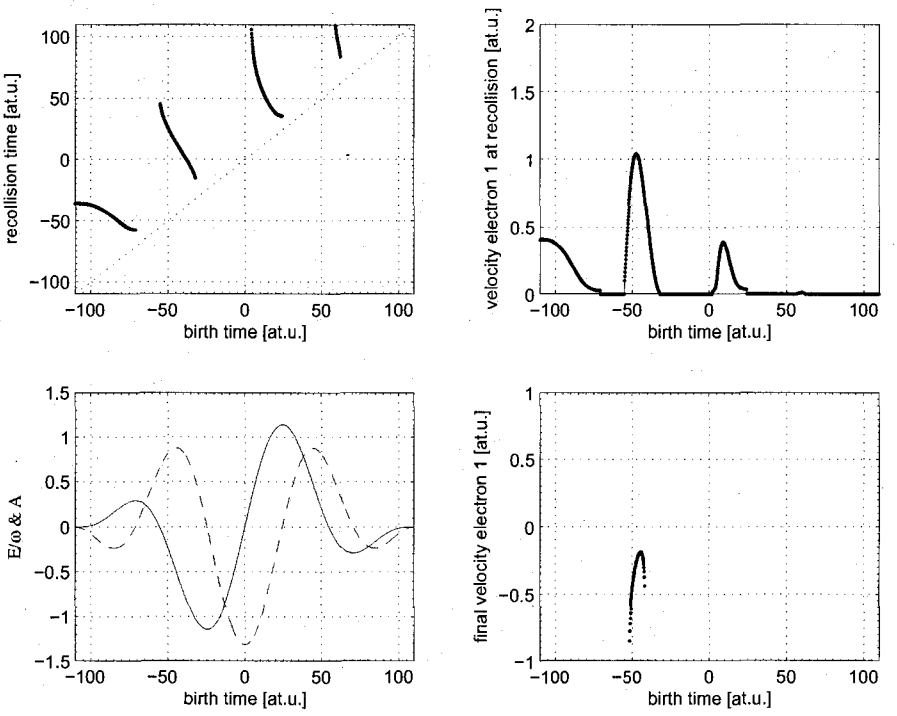

Figure 5.4. Top left: Recollision time (τ_r) as a function of birth time (τ_b). Top right: Energy of the returning electron as a function of τ_b. Bottom left: The vector potential (solid line) and electric field (dashed line). Bottom right: Final energy of the first electron as a function of birth time for the first excited state.

excited state, the excited electron is ionized by ABI and aquires a drift velocity of $A(\tau_b')$ at the end of the pulse. This process is examined for the first, second and third excited states. The process where the returning electron immediately ionizes the second electron was not considered.

In figure 5.4 it can be seen that the highest return energy is approximately 1.1 which corresponds to the ionization potential of N_2^+; this shows that immediate ionization by the returning electron does not contribute significantly to the double ionization. In the plot of the return energy vs τ_b we can see two peaks. Electrons with the highest return energies are born near the peak of the pulse around $\tau = -50$. These electrons return to the nucleus slightly before the next peak at $\tau = 0$, excite the bound electron and continue in the negative x-direction. From $\tau = 0$ to the end of the pulse the bound electron is ionized when the barrier suppression is large enough to cause ABI. When the vector potential is positive the second electron's final momentum will be in the same direction as the first and when the vector potential is negative its momentum will be in the opposite direction. Furthermore, in the range over which this ionization process takes place the vector potential takes on larger positive values (in magnitude) than negative ones. Hence we would expect that the second electron will have a larger range of negative final momenta.

The second peak in the top right of figure 5.4 is a result of the first electron being born near the peak around $\tau = 0$. These electrons return around $\tau = 50$ where the pulse has another peak. However, the return energy of these electrons is much smaller than those born around the peak at $\tau = -50$. Upon return, these elctrons do not have enough energy to cause the bound electron to move to an excited state and thus classically do not play a role in the double ionization. As such, we assume a constant ionization rate for electrons ionized near $\tau = -50$ and do not consider the trajectories of electrons born near $\tau = 0$.

This is precisely what is seen in figure 5.5 where we have plotted the momentum components parallel to the field direction ($k^{\parallel}_{1,2}$) for each electron at the end of the pulse. We see a fairly small range of momenta occuring in quadrants two and four where the electrons have momenta in the opposite directions, and a significantly larger mometum range in quadrant three where the electrons move in the same direction. Most of the ionization events seen in figure 5.5 lie on the main "cross" shaped region. The narrowness of the lines making up the "cross" can be explained by the plot in the bottom right corner of figure 5.4. Here we see return energies of the first electron that are high enough to bring the bound electron to the first excited state. It can be seen that most of the events that will cause this excitation are densely clustered in a very narrow energy range. Thus, we would expect that most of the final momenta of the recolliding electron also lie in a narrow range. On the other hand the second electron can be ionized at many different times until the end of the pulse and thus we expect it to have a much larger range of final momenta. So, to reiterate, the thickness and postition of the lines that make up the "cross" are determined by return energies of recolliding electron and the length is determined by the range of drift velocities given to the second electron by the field. The symmetries in figure 5.5 are due to the indistinguishability of the two electrons.

5.2.2 The MCTDHF calculations

In the MCTDHF calculations we consider two cases: i) when the molecule is aligned parallel to the pulse direction and ii) when the molecule is aligned perpendicular to the pulse direction. The electron-electron shielding a is given by $a = 0.74$. a and b were chosen so that the ionization potential I_p was close to the ionization potential of N_2 ($I_p = 0.551$).

Calculations were done using increasing numbers of configurations ($n = 6$, 8, 10, 12 and 14) in the box $B = [-100, 100] \times [-50, 50]$ with uniform grid spacings $\Delta x = 0.39$ and $\Delta y = 0.78$. At the end of each pulse we calculate the single, double and total ionization probabilities in a manner similar to that of reference [90]. The bound region B_b, the double ionization channel B^{++} and the single ionization channel B^{+} are given by,

$$B_b = \{(x_j, y_j) \,|\, |x_j|, |y_j| > \epsilon\} \tag{5.10}$$

$$B^{++} = \{(x_j, y_j) \,|\, |x_j|, |y_j| < \epsilon\} \tag{5.11}$$

$$B^{+} = B \setminus (B_b \cup B^{++}) \tag{5.12}$$

where ϵ is the maximum extension of the ground state along the coordinate axis. By defining the functional $I_{\eta\zeta}$ to be,

$$I_{\eta\zeta}[f] = \int_{-\eta}^{\eta}\int_{-\eta}^{\eta}\int_{-\zeta}^{\zeta}\int_{-\zeta}^{\zeta} |f(x_1, y_1, x_2, y_2)|^2 dx_1 dy_1 dx_2 dy_2 \tag{5.13}$$

where $f : \mathbb{R}^4 \to \mathbb{C}$, we have the following expression for the total ionization probability P_T:

$$P_T = I_{\infty\infty}[\Psi] - I_{\epsilon\epsilon}[\Psi] \tag{5.14}$$

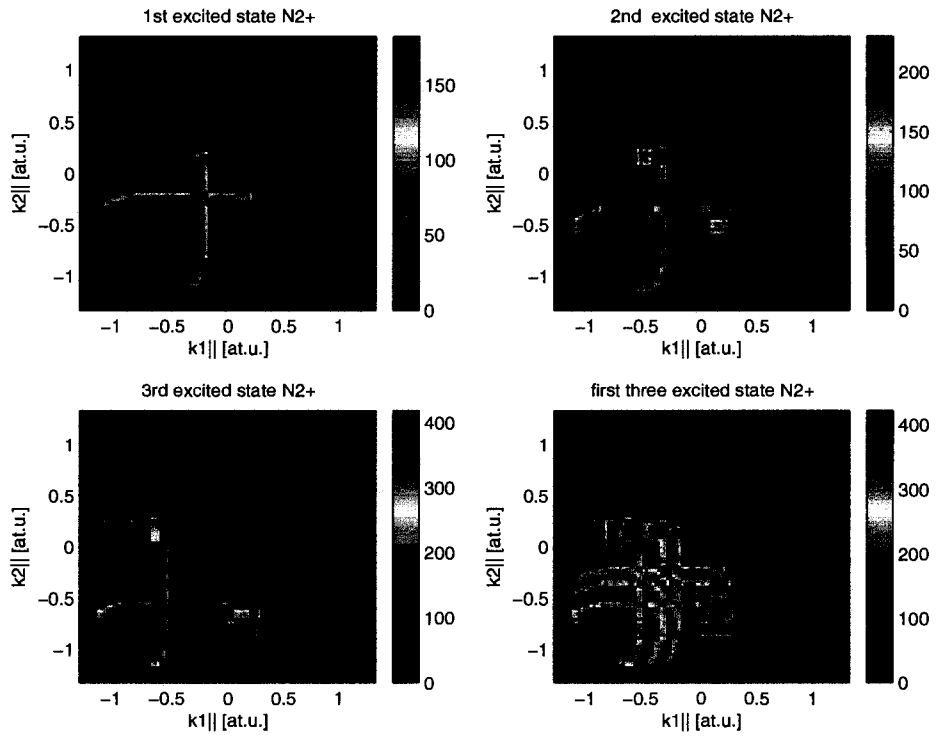

Figure 5.5. Momentum correlation maps at the end of the laser pulse for electrons resulting from excitation to the first (top left), second (top right) and third (bottom left) excited states. The bottom right plot shows the resulting momentum correlation map when all three excited states are taken into consideration.

The double-ionization probability P^{++} is determined from,

$$P^{++} = I_{\infty\infty}[\Psi] - I_{\infty\epsilon}[\Psi] - I_{\epsilon\infty}[\Psi] + I_{\epsilon\epsilon}[\Psi] \tag{5.15}$$

and the single-ionization probability P^{+} is then determined by,

$$P^{+} = P_T - P^{++}. \tag{5.16}$$

Tables 5.1 and 5.2 show the calculated single, double and total ionization probabilities at the end of the pulse for parallel and perpendicular alignment respectively. The numbers in tables 5.1 and 5.2 clearly show that there is more ionization for molecules aligned parallel to the pulse polarization direction and thus agree (at least qualitatively) with what has been found experimentally.

In order to get a picture of the dynamics involved in the ionization process we use the first order density function given by,

$$\rho_1(x_1, y_1; t) = \int |\Psi(x_1, y_1, x_2, y_2)|^2 dx_2 dy_2. \tag{5.17}$$

n	$\binom{n}{2}$	P^+	P^{++}	P_T	$E_0(N_2)$
6	15	0.09816	0.00149	0.09964	-1.6404
8	28	0.13049	0.00065	0.13114	-1.6438
10	45	0.13096	0.00106	0.13201	-1.6441
12	66	0.13150	0.00097	0.13247	-1.6444
14	91	0.12977	0.00084	0.13061	-1.6446

Table 5.1. Calculated single, double and total ionization probabilities for N_2 with its molecular axis aligned parallel to the field polarization direction. $E_0(N_2)$ is the ground state energy of the N_2 molecule in atomic units.

n	$\binom{n}{2}$	P^+	P^{++}	P_T	$E_0(N_2)$
6	15	0.08079	0.00183	0.08262	-1.6363
8	28	0.09128	0.00052	0.09180	-1.6397
10	45	0.09133	0.00077	0.09209	-1.6400
12	66	0.09149	0.00054	0.09203	-1.6403

Table 5.2. Calculated single, double and total ionization probabilities for N_2 with its molecular axis aligned perpendicular to the field polarization direction. $E_0(N_2)$ is the ground state energy of the N_2 molecule in atomic units.

Also, to observe the correlated motion of the two electrons in the direction parallel to the laser-electric field, we calculate the two-electron $\rho_2(x_1, y_1, x_2, y_2)$ density and integrate over the coordinates perpendicular to the field to get $\rho_2^{\parallel}$. This is given by,

$$\rho_2^{\parallel}(x_1, x_2) = \int |\Psi(x_1, y_1, x_2, y_2)|^2 dy_1 dy_2. \tag{5.18}$$

Figures 5.6 and 5.7 show ρ_1 and $\rho_2^{\parallel}$ at times $\tau = -27$, 3, 23, 53 and 63 (top to bottom) in the laser-electric field with the molecular axis aligned parallel to the field. The first plot at $\tau = -27$ occurs shortly after ionization begins. In the plot of ρ_1 we see a shift of probability along the positive x-direction. For the plot of $\rho_2^{\parallel}$ we don't yet see any correlated motion. In the next plot we see ρ_1 just shortly after the centre of the pulse ($\tau = 0$). Here the ionized electrons are returning to the nucleus. As well, in the classical model, electrons could also be ionized around $\tau = 0$; we see this occuring due to a shift of probability along the negative x-direction; this might also contain some of the recolliding and second ionized electrons. It also should be noted that in the plot of $\rho_2^{\parallel}$ we are begining to see some correlated motion in the third quadrant.

In the third graph we see a significant amount of probability shifted along the negative x-direction. This is a result of the first recolliding electron and the electrons ionized around $\tau = 0$ travelling in this direction. The wave structure we see developing is most likely as a result of interference between these electrons. Observing $\rho_2^{\parallel}$ we see more probability developing in quadrant three as a result of the second ionized electron having its momentum in the same direction as that of the recolliding electron. Also, in quadrants two and four we see some probability developing. This is a result of the second electron moving in the opposite direction of the recolliding electron.

In the fourth and fifth plots of $\rho_2^{\parallel}$ we can see quite a bit of correlated motion in quadrant three. We can also observe "bar" structures perpendicluar to the positive $x_{1,2}^{\parallel}$-axis. As we go from $\tau = 53$ to $\tau = 63$ we see these "bars" move in the positive direction and then dissipate. This is a result of the recolliding electrons born around $\tau = 0$ moving away from the ion after recollision. When these "lines" start to disappear we begin to see correlated motion in quadrant one which we should not see classically. Below we will provide a reason for why this occurs.

In order to compare the MCTDHF results with the results of the classical model we also plot a momentum correlation map for the doubly ionized electrons using the $n = 14$ result. This map is a plot of $k_{x_1}^{\parallel}$ vs $k_{x_2}^{\parallel}$ with the bound states and the single-ionization channel filtered out. To obtain this map we apply the filter function $w_m(x_1, y_1, x_2, y_2, \Delta)$ given by,

$$w_m(x_1, y_1, x_2, y_2, \Delta) = \prod_{j=1}^{2} (1 - G_m(x_j, y_j, \Delta)) \tag{5.19}$$

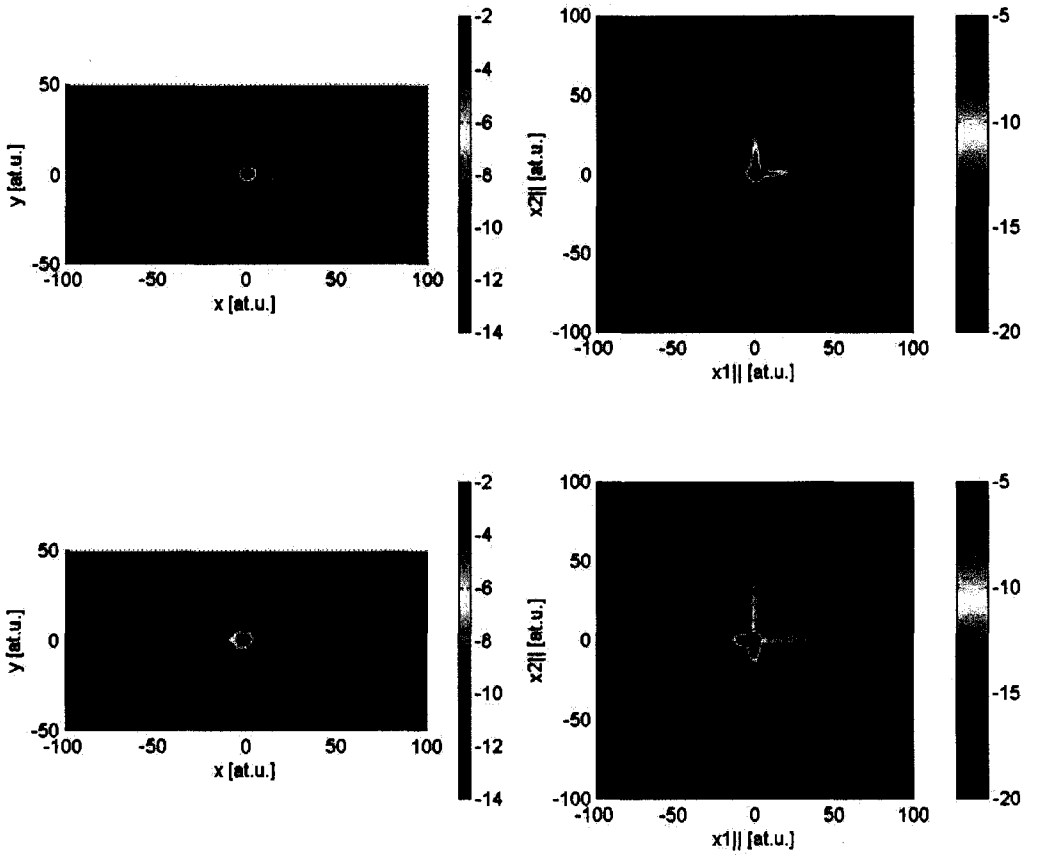

Figure 5.6. Log plots of ρ_1 and $\rho_2^{\parallel}$ for $\tau = -27$ and 3 (top to bottom).

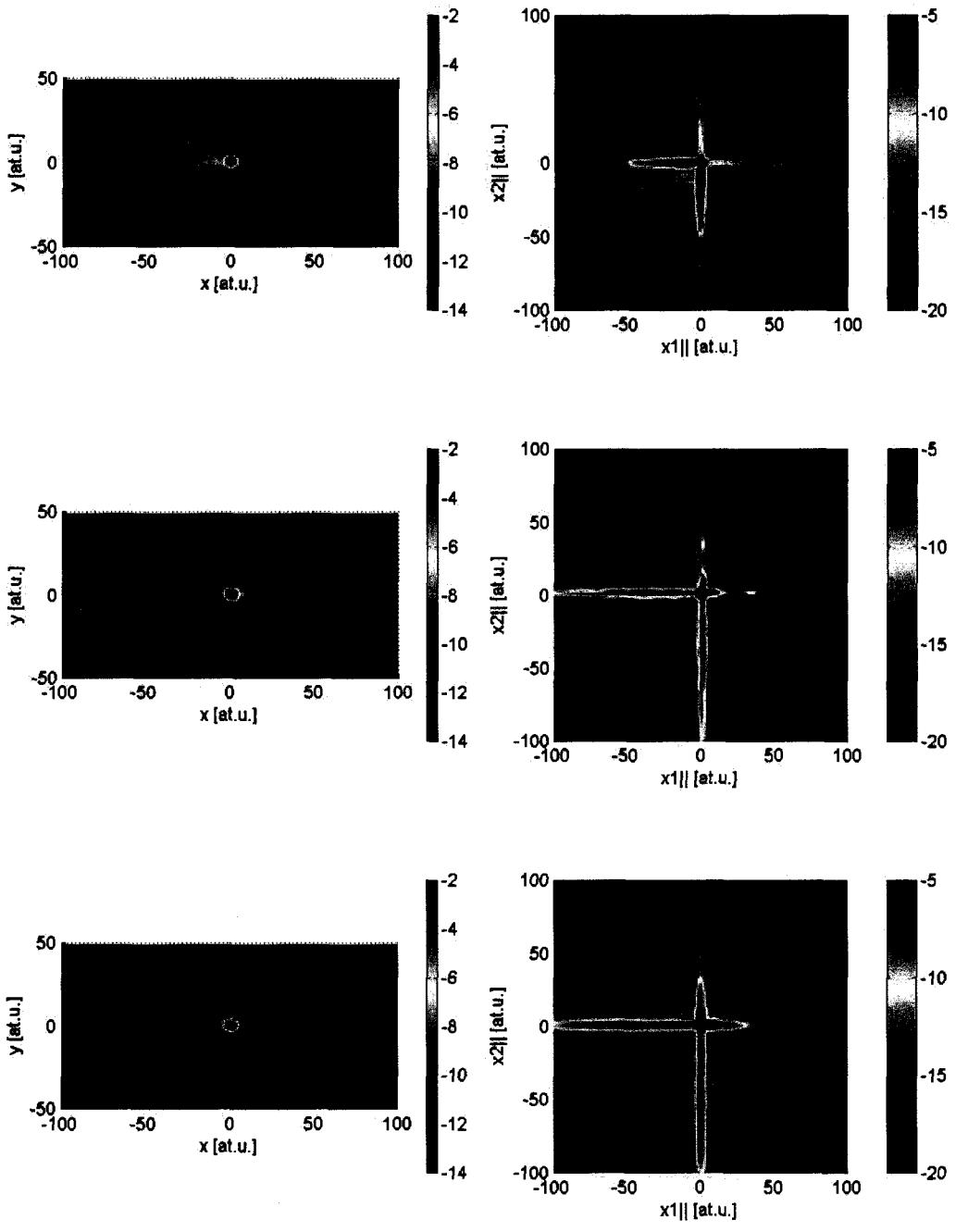

Figure 5.7. Log plots of ρ_1 and $\rho_2^{\parallel}$ for $\tau = 23$, 53 and 63 (top to bottom).

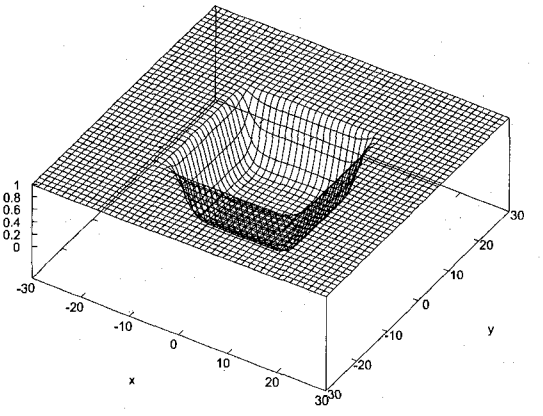

Figure 5.8. Surface plot of $(1 - G_{10}(x, y, 12))$.

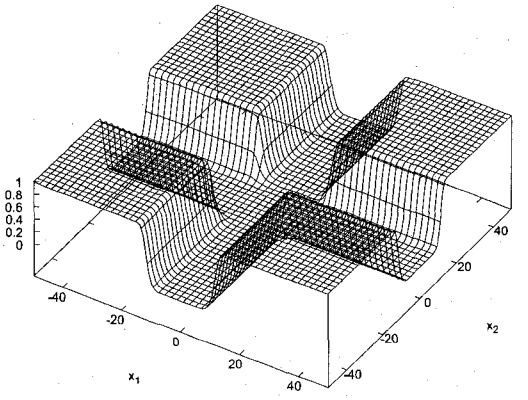

Figure 5.9. Surface plot of $w_{10}(x_1, 0, x_2, 0, 12)$.

where G_m is given by,

$$G_m(x, y, \Delta) = \exp\left[-\left(\frac{x}{\Delta}\right)^m\right] \cdot \exp\left[-\left(\frac{y}{\Delta}\right)^m\right] \tag{5.20}$$

with $m \in \mathbb{I}^+$ and $\Delta \in \mathbb{R}$ giving the width of the filter; in our filter we use $m = 10$ and $\Delta = 12$. Figure 5.8 shows a 3-D surface plot of $(1 - G_{10}(x, y, 12))$ and figure 5.9 gives 3-D surface plot of $w_{10}(x_1, 0, x_2, 0, 12)$. When applied to the electron wave function it is clear the bound state and the single-ionization channels will be supressed.

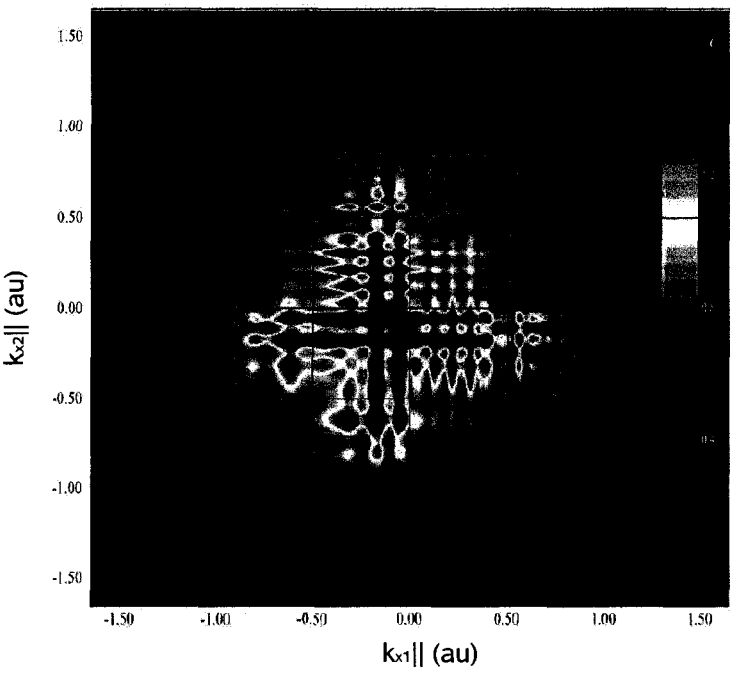

Figure 5.10. Momentum correlation map of $k_{x_1}^{\|}$ vs $k_{x_2}^{\|}$ for the MCTDHF calculation with $n = 14$. In this calculation the molecular axis was aligned parallel to the laser-electric field. The number labels on the colour scale are all $\times 10^{-2}$ au.

To obtain the electron momentum correlation map we apply the filter to the wave function in order to obtain the doubly ionized part Ψ^{2+}; that is,

$$\Psi^{2+}(x_1, y_1, x_2, y_2) = w(x_1, y_1, x_2, y_2) \cdot \Psi(x_1, y_1, x_2, y_2). \tag{5.21}$$

We then take the Fourier of transform Ψ^{2+} to get $\tilde{\Psi}^{2+}(k_1, k_1, k_2, k_2)$. The correlation map for the momentum components parallel to the field direction is then obtained from,

$$|\tilde{\Psi}_{\|}^{2+}(k_{x_1}, k_{x_2})|^2 = \int\int dk_{y_1} dk_{y_2} |\tilde{\Psi}^{2+}(k_{x_1}, k_{y_1}, k_{x_2}, k_{y_2})|^2. \tag{5.22}$$

In figure 5.10 we show the contour plot of $|\tilde{\Psi}_{\|}^{2+}|^2$. It can be seen right away that this bears a striking resemblance to the plots in figure 5.5. We can clearly see the "cross" shapes produced by ABI of electrons in the first, second and third excited states. As well, we can see that the momentum range is larger in quadrant three than in quadrants two and four. By comparing figures 5.5 and 5.10 it is clear that we observe all classical effects in our quantum mechanical calculations. There are, however, some significant differences that cannot be explained classically.

One major difference between what is seen in figures 5.5 and 5.10 is that in figure 5.10 there are some final momenta in the first quadrant indicating that the recolliding electron was moving

in the positive x-direction at the time of recollision. According to figure 5.4 this will occur for the first electron being born around $\tau = 0$. Classically, when these electrons return they do not have enough energy to cause the bound electron to move to an excited state. This can be explained due to a Stark shift of the N_2^+ ground and excited states. In terms of polarizability α and field amplitude $|E|$, the Stark shift ΔE is given by,

$$\Delta E = \frac{\alpha}{2}|E|^2. \tag{5.23}$$

The polarizability of the ground and first excites states of N_2^+ are $\alpha_0 \sim 20$ and $\alpha_1 \sim 200$ respectively. This indicates that there will be a significant lowering of the first excited state relative to the ground state. Thus, with the reduced spacing between these states it is possible for the bound electron to become excited by the lower energy returning electrons. Then, upon sufficient barrier suppression, the second electron is ionized above barrier.

Also, in figure 5.10 it can be observed that the bars making up the "cross" structures are shifted relative to the corresponding ones in figure 5.5. This is also a result of the Stark shift since the final velocity of the recolliding electron depends on the energy spacing between the ground and excited state.

What information can we gather from examining the momentum correlation plots at the end of the pulse? First, since each excited state corresponds to a unique position of its cross structure, it is possible to determine which laser dressed excited state the second electron was in at the time of ionization. Secondly, by examining the final momenta of the electrons we are able to determine their birth times. These calculations provide a way to characterizes the attosecond dynamics of atoms and molecules without using attosecond pulses.

Chapter 6

Conclusion

We have presented the multi-configuration time-dependent Hartree-Fock (MCDTHF) method for multielectron systems in a time-dependent external field. A full derivation of the MCTDHF equations of motion was given and it was shown how the more complicated the portions of the calculation (ie: the mean-field) can be simplified. From a computational standpoint MCTDHF has some very favorable properties:

(i) For f electrons, MCTDHF scales linearly with number of spin-orbital functions $n \geq f$ and as $\binom{n}{f}$ for the expansion coefficients; the scaling is independent of the dimension of the problem being considered. This is in contrast to the exponential scaling with the number of electrons for straight forward discretization of the TDSE.

(ii) In contrast to TDHF, MCTDHF uses more more than one Slater determinant to approximate the quantum mechanical wave function. Furthermore, the expansion functions and coefficients are optimized by a varitaional principle. Thus, good convergence can be reached without an unmanageable amount of configurations as with the CI approach.

We have developed a computer code to solve the MCTDHF equations of motion using the C programming language. The code is capable of solving the TDSE for small 2-D multielectron systems as well as larger 1-D systems on single processor machines in a reasonable time period. The code is written in such a way that it can be easily expanded to three dimensions and once a parallelized version of the code is finished it will be capable performing calculations on 3-D systems. In addition we have written several post-processing routines to extract the relevant physics from the wave function; these include energies, electron densities, ionization probabilities and electron momentum correlation maps.

The MCTDHF program was used to investigate the ionization dynamics of N_2 in the presence of a strong laser-electric field using a 2-D, N_2 molecule. Two cases were considered: (i) N_2 with its molecular axis parallel to the laser-electric field and (ii) N_2 with its molecular axis perpendicular to the field. The molecule was subjected to a linearly polarized laser pulse of intensity $2 \times 10^{14}\, W/cm^2$ and wavelength 800 nm. The calculation was done for two cycles of the vector potential, in a sine square envelope, over a period of 5.2 fs. The results showed that there was more ionization when the molecule was alligned parallel, as opposed to perpendicular, to the direction of the field polarization. These results are in agreement with what has been observed experimentally.

We also presented a more detailed investigation for the case with the molecular axis aligned parallel to the field direction. We presented a classical model for the ionization dynamics of our system and compared it with our quantum mechanical results. Most of our quantum mechanical

observation were able to be explained within the framework of our classical model. However, in our correlation plots we did observe events occuring in quadrant one that are not explained by the classical model. Based on the polarizability of the ground and first excited states of we have proposed a mechanism where ionization is possible due to a decrease in the energy spacing between these states. These results provide a means for characterizing the attosecond dynamics of atoms and molecules without using attosecond pulses.

Appendix A

Conversion between SI and atomic units

Since atomic units are not commonly used, this appendix gives the conversion between SI and atomic units. Here the abbreviation "au" is used for atomic unit.

(i) Charge: 1 au = 1.602×10^{-19} C
(ii) Length: 1 au = 0.52918×10^{-8} cm
(iii) Mass: 1 au = 9.109×10^{-31} kg
(iv) Energy: 1 au = 4.3597×10^{-18} J
(v) Time: 1 au = 2.4189×10^{-17} s
(vi) Electric Potential: 1 au = 27.211 V
(vii) Electric Field Strength: 1 au = 5.1422×10^{11} V/m

References

[1] M. Kitzler, J. Zanhellini, Ch. Junreuthmeyer, M. Smits, A. Scrinzi, and T. Brabec. Ionization dymanics of extended multielectron systems. *Phys. Rev. A*, 70:041401(R), October 2004.

[2] R. Kienberger et al. Steering attosecond electron wave packets with light. *Science*, 297:1144, 2002.

[3] M. Drescher et al. Time-reolved atomic inner-shell spectroscopy. *Nature*, 419:803, 2002.

[4] S.M. Hankin et al. Nonlinear ionization of organic molecules in high intensity laser fields. *Phys. Rev. Lett.*, 91(20):203004, November 2003.

[5] M. Lezius et al. Nonadiabatic multielectron dymanics in strong field molecular ionization. *Phys. Rev. Lett.*, 86(1):51, January 2001.

[6] P.B. Corkum V.R. Bhardwaj and D.M. Rayner. Internal laser-induced dipole force at work in C_{60} molecule. *Phys. Rev. Lett.*, 91(20):203004, November 2003.

[7] A. Szabo and N.S. Ostlund. *Modern Quantum Chemistry: Introduction ot Adavanced Electronic Structure Theory.* McGraw-Hill, New York, 1st Rev. edition, 1989.

[8] K.C. Kulander. Time-dependent hartree-fock theory of multiphoton ionization: Helium. *Phys. Rev. A*, 36(6):2726, September 1987.

[9] K.C. Kulander. Time-dependent theory of multiphoton ionization of xenon. *Phys. Rev. A*, 38(2):778, July 1988.

[10] M. S. Pindzola, D.C. Griffin, and C. Bottcher. Validity of the time-dependent Hartree-Fock theory for multiphoton ionization of atoms. *Phys. Rev. Lett.*, 66(18):2305, May 1991.

[11] M. S. Pindzola, T. W. Gorczyca, and C. Bottcher. Two-photon ionization of lithium in the time-dependent Hartree-Fock approximation. *Phys. Rev. A*, 47(6):4982, June 1993.

[12] M. S. Pindzola, P. Gavras, and T. W. Gorczyca. Time-dependent unrestriced Hartree-Fock theory for multiphoton ionization of atoms. *Phys. Rev. A*, 51(5):3999, May 1995.

[13] M. S. Pindzola, F. Robicheaux, and P. Gavras. Double multiphoton ionization of a model atom. *Phys. Rev. A*, 55(2):1307, February 1997.

[14] N.E. Dahlen and R. van Leeuwen. Double ionization of a two-electron system in the time-dependent extended Hartree-Fock approximation. *Phys. Rev. A*, 64:023405, July 2001.

[15] H.J. Kull and D. Pfirsch. Generalized variational principle for the time-dependent Hartree-Fock equations for a Slater determinant. *Phys. Rev. E*, 61(5):5940, May 2000.

[16] S.P. Goldman. Modified Configuration Interaction Method for Accurate Calculations with Small Basis Sets. *Phys. Rev. Lett.*, 73(19):2547, November 1994.

[17] R.R. Chasman. Variational Appraoch to Configuration Interaction. *Phys. Rev. Lett.*, 95:262501, December 2005.

[18] P. Hohenberg and W. Kohn. Inhomogeneous Electron Gas. *Phys. Rev.*, 136(3B):B864, November 1964.

[19] W. Kohn. Nobel Lecture: Electronic structure of matter - wave functions and density functionals. *Rev. Mod. Phys.*, 71(5):1253, October 1999.

[20] W. Kohn and L.J. Sham. Self-consisent Equations Including Exchange and Correlation Effects. *Phys. Rev.*, 140:A1133, November 1965.

[21] E. Runge and E.K.U. Gross. Density Functional Theory for Time-Dependent Systems. *Phys. Rev. Lett.*, 52(12):997, March 1984.

[22] R. van Leeuwen. Mapping from Densities to Potentials in Time-Dependent Density-Functional Theory. *Phys. Rev. Lett.*, 82(19):3863, May 1999.

[23] N.A. Nguyen and Andre D. Bandrauk. Electron correlation of one-dimensional H_2 in intense laser fields: Time-dependent extended Hartree-Fock and time-dependent density-functional theory approaches. *Phys. Rev. A*, 73:032708, March 2006.

[24] A. Görling and M. Levy. Exact Kohn-Sham scheme bases on perturbation theory. *Phys. Rev. A*, 50(1):196, July 1994.

[25] M. Seidl, J.P. Perdew, and S. Kurth. Simulation of All-Order Density-Functional Perturbation Theory, Using the Second Order and the StrongCorrelation Limit. *Phys. Rev. Lett.*, 84(22):5070, May 2000.

[26] N. T. Maitra and K. Burke. Memory in Time-Dependent Density Functional Theory. *Phys. Rev. Lett.*, 89(2):023002, July 2002.

[27] Zheng-Li Cai, K. Sendt, and J. R. Reimers. Failure of density-functional theory and time-dependent density-functional theory for large extended π systems. *J. Chem. Phys.*, 117(12):5543, September 2002.

[28] M. Stener, P. Decleva, and A. Görling. The role of exchange and correlation in time-dependent density-functional theory for photoionization. *J. Chem. Phys.*, 114(18):7816, May 2001.

[29] H.-D. Meyer, U. Manthe, and L.S. Cederbaum. The Multi-configurational Time-dependent Hartree Approach. *Chem. Phys. Lett.*, 165(1):73, 1990.

[30] M. H. Beck, A. Jäckle, G. A. Worth, and H.-D. Meyer. The multiconfiguration time-dependent Hartree (MCTDH) method: A highly efficient algorithm for propagating wavepackets. *Physics Report*, 324(1):1, January 2000.

[31] P. A. M. Dirac. *Proc. Cambridge Philos. Soc.*, 26:376, 1930.

[32] J. Frenkel. *Wave Mechanics*. Clarendon Press, Oxford, 1934.

[33] A.D. McLachlan. A variational solution of the time-dependent Schrödinger equation. *Mol. Phys.*, 8:39–44, 1964.

[34] G. A. Worth, H.-D. Meyer, and L. S. Cederbaum. The effect of a model environment on the S_2 absorption spectrum of pyrazine: A wave packet study treating all 24 vibrational modes. *J. Chem. Phys.*, 105(11):4412, September 1996.

[35] G. A. Worth, H.-D. Meyer, and L. S. Cederbaum. Relaxation of a system with a conical intersection coupled to a bath: A benchmark 24-dimensional wave packet study treating the environment explicitly. *J. Chem. Phys.*, 109(9):3518, September 1998.

[36] A. Raab, G. A. Worth, H.-D. Meyer, and L. S. Cederbaum. Molecular dynamics of pyrazine after excitation to the S2 electronic state using a realistic 24-mode model Hamiltonian. *J. Chem. Phys.*, 110(2):936, January 1999.

[37] U. Manthe, H.-D. Meyer, and L. S. Cederbaum. Multiconfigurational time-dependent Hartree study of complex dynamics: Photodissociation of NO_2. *J. Chem. Phys.*, 97(12):9062, December 1992.

[38] A.D. Hammerich, U. Manthe, and R. Kosloff. Time-dependent photodissociation of methyl iodide with five active modes. *J. Chem. Phys.*, 101(7):5623, October 1994.

[39] L. Liu, J.-Y. Fang, and H. Guo. How many configurations are needed in a time-dependent Hartree treatment of the photodissociation of ICN? *J. Chem. Phys.*, 102(6):2404, February 1994.

[40] A. Capellini and A.P.J. Jansen. Convergence study of multi-configuration time-dependent Hartree simulations: H_2 scattering from LiF(001). *J. Chem. Phys.*, 104(9):3366, March 1996.

[41] M. Ehara, H.-D. Meyer, and L. S. Cederbaum. Multiconfiguration time-dependent Hartree (MCTDH) study on rotational and diffractive inelastic molecule-surface scattering. *J. Chem. Phys.*, 105(19):8865, November 1996.

[42] R. Milot and A. P. J. Jansen. Ten-dimensional wave packet simulations of methane scattering. *J. Chem. Phys.*, 109(5):1966, August 1998.

[43] J. Zanhellini, M. Kitzler, C. Fabian, T. Brabec, and A. Scrinzi. An MCTDHF Appraoch to Multi-electron Dynamics in Laser Fields. *Laser Phys.*, 13(8):1064, 2003.

[44] B. Walker, B. Sheehy, L. F. DiMauro, P. Agostini, K. J. Schafer, and K. C. Kulander. Precision Measurement of Strong Field Double Ionization of Helium. *Phys. Rev. Lett.*, 73(9):1227, August

1994.

[45] A. S. Alnaser et al. Rescattering Double Ionization of D_2 and H_2 by Intense Laser Pulses. *Phys. Rev. Lett.*, 91(16):163002, October 2003.

[46] A. Rudenko et al. Correlated Multielectron Dynamics in Ultrafast Laser Pulse Interactions with Atoms. *Phys. Rev. Lett.*, 93:253001, December 2004.

[47] T. Brabec, M. Yu, and P.B. Corkum. Coulomb focusing in intense field atomic processes. *Phys. Rev. A*, 54(4):R2551, October 1996.

[48] Phay J. Ho and J.H. Eberly. Classical Effects of Laser Pulse Duration on Strong-Field Double Ionization. *Phys. Rev. Lett.*, 95:193002, November 2005.

[49] F.H.L. Koppens et al. Driven coherent oscillations of a single electron spin in a quantum dot. *Nature*, 442:766, 2006.

[50] H. Park. Nanomechanical oscillations in a single-C60 transistor. *Nature*, 407:57, 2000.

[51] J. Bylander, T. Duty, and P. Delsing. Current measurement by real-time counting of single electrons. *Nature*, 434:361, 2005.

[52] J. Caillat, J. Zanghellini, M. Kitzler, O. Koch, W. Kreuzer, and A. Scrinzi. Correlated multielectron systems in strong laser fields: A multiconfiguration time-dependent Hartree-Fock approach. *Phys. Rev. A*, 71:012712, January 2005.

[53] J. Zanhellini, M. Kitzler, T. Brabec, and A. Scrinzi. Testing the multi-configuration time-dependent Hartree-Fock method. *J. Phys. B: At. Mol. Opt. Phys.*, 37:763, January 2004.

[54] Z. Zhang, C.F. Destefani, C. McDonald, and T. Brabec. Transport properties of nanodevices: A one-dimensional model study. *Phys. Rev. B*, 72:161309(R), October 2005.

[55] I.P. Christov. Time-dependent quantum Monte-Carlo: preparation of the ground state. (Not yet published).

[56] B. Hammond, W. Lesler, and P. Reynolds. *Monte Carlo Methods in Ab Initio Quantum Chemistry.* World Scientific, Singapore, 1994.

[57] I.P. Christov. Correlated non-perturbative electron dynamics with quantum trajectories. *Opt. Express*, 14(15):6906, July 2006.

[58] I.P. Christov. Quantum trajectory perspective of atom-field interaction in attosecond time scale. *Appl. Phys. B*, 85:503, September 2006.

[59] P. Holland. *The Quantum Theory of Motion.* Cambridge University Press, Cambridge, 1993.

[60] Christian Lubich. A variational splitting integrator for quantum molecular dynamics. *App. Num. Math.*, 48:355–368, 2004.

[61] D. Kincaid and Ward Cheney. *Numerical Analysis: Mathematics of Scientific Computing.* Brooks/Cole, Pacific Grove, CA, 3rd edition, 2002.

[62] K. Gottfried and T. Yan. *Quantum Mechanics: Fundamentals.* Springer-Verlag, New York, 2nd edition, 2003.

[63] Mary L. Boas. *Mathematical Methods in the Physical Sciences.* John Wiley & Sons, Inc., 2nd edition, 1983.

[64] T. Kato and H. Kono. Time-dependent multiconfiguration theory for dymanics of molecules in an intense laser field. *Chem. Phys. Lett.*, 392:533–540, 2004.

[65] M. Nest, T. Klamroth, and P. Saalfrank. The multiconfiguration time-dependent Hartree-Fock method for quantum chemical calculations. *J. Chem. Phys.*, 122:124102, 2005.

[66] T.A. Driscoll. A composite Runge-Kutta method for the spectral solution of semilinear PDEs. *J. Comp. Phys.*, 182:357–367, 2002.

[67] P.B. Corkum. Above-Threshold Ionization in the Long-Wavelength Limit. *Phys. Rev. Lett.*, 62(11):1259, March 1989.

[68] P.B. Corkum. Plasma Perspective on Strong-Field Multiphoton Ionization. *Phys. Rev. Lett.*, 71(13):1994, September 1993.

[69] L.V. Keldysh. Ionization in the field of a strong electromagnetic wave. *Sov. Phys. - JETP*, 20:1307, 1965.

[70] T. Brabec and F. Krausz. Intense few-cycle laser fields: Frontiers of nonlinear optics. *Rev. Mod. Phys.*, 72(2):545, April 2000.

[71] P. Mulser, S. Uryupin, R. Sauerbrey, and B. Wellegehausen. Ponderomotive potential and dynamical Stark shift in multiphoton ionization. *Phys. Rev. A*, 48(6):4547, December 1993.

[72] M. Lewnestein et al. Theory of high-harmonic generation by low-frequency laser fields. *Phys. Rev. A*, 49(3):2117, March 1994.

[73] K.J. Schafer, B. Yang, L.F. DiMauro, and K.C. Kulander. Above Threshold Ionization Beyond the High Harmonic Cutoff. *Phys. Rev. Lett.*, 70(11):1599, March 1993.

[74] X.M. Tong, Z.X. Zhao, and C.D. Lin. Theory of molecular tunneling ionization. *Phys. Rev. A*, 66:033402, September 2002.

[75] M. V. Ammosov, N. B. Delone, and V. P. Krainov. Tunnel ionization of complex atoms and of atomic ions in an alternating electromagnetic field. *Sov. Phys. - JETP*, 64:1191, 1986.

[76] S. Augst et al. Tunneling Ionization of Noble Gases in a High-Intensity Laser Field. *Phys. Rev. Lett.*, 63(20):2212, November 1989.

[77] A. Scrinzi, M. Geissler, and T. Brabec. Ionization Above the Coulomb Barrier. *Phys. Rev. Lett.*, 83(4):706, July 1999.

[78] M.Y. Ivanov, T. Brabec, and N. Burnett. Coulomb corrections and polarization effects in high-intensity high-harmonic emision. *Phys. Rev. A*, 54(1):742, July 1996.

[79] A. l'Huillier, L. A. Lompre, G. Mainfray, and C. Manus. Multiply charged ions induced by multiphoton absorption in rare gases at 0.53 μm. *Phys. Rev. A*, 27(5):2503, May 1983.

[80] D.N. Fittinghoff, P.R. Bolton, B. Chang, and K.C. Kulander. Observation of Nonsequential Double ionization of Helium with Optical Tunneling. *Phys. Rev. Lett.*, 69(18):2642, November 2000.

[81] U. Eichmann et al. Collective Multielectron Tunneling Ionization in Strong Fields. *Phys. Rev. Lett.*, 84(16):3550, April 2000.

[82] J.B. Watson et al. Nonsequential Double Ionization of Helium. *Phys. Rev. Lett.*, 78(10):1884, March 1997.

[83] Th. Weber et al. Recoil-Ion Momentum Distributions for Single and Double Ionization of Helium in Strong Laser Fields. *Phys. Rev. Lett.*, 84(3):443, January 2000.

[84] R. Moshammer et al. Momentum Distributions of nc^{n+} Ions Created by an Intense Ultrashort Laser Pulse. *Phys. Rev. Lett.*, 84(3):447, January 2000.

[85] Th. Weber et al. Correlated electron emission in multiphoton double ionization. *Nature*, 405:658, 2000.

[86] B. Feuerstein et al. Separation of recollision mechanisms in nonsequential double ionization of Ar: The role of excitation tunneling. *Phys. Rev. Lett.*, 87(4):043003, July 2001.

[87] M. Weckenbrock et al. Fully differential rates for femtosecond multiphoton double ionization of neon. *Phys. Rev. Lett.*, 92(21):213002, May 2004.

[88] I.V. Litvinuk et al. Alignment-Dependent Strong Field Ionization of Molecules. *Phys. Rev. Lett.*, 90(23):233003, June 2003.

[89] D. Zeidler, A. Staudte, A.B. Bardon, D.M. Villeneuve, R. Dörner, and P.B. Corkum. Controlling attosecond double ionization dynamics via molecular alignment. *Phys. Rev. Lett.*, 95:203003, November 2005.

[90] D. Bauer. Two-dimensional, two-electron model atom in a laser pulse: Exact treatment, single-active electron analysis, time-dependent density functional theory, classical calculations and nosequential ionization. *Phys. Rev. A*, 56(4):3028, October 1997.